Photoemission and the Electronic Structure of Transition Metal Compounds

J. ZAANEN*) and G. A. SAWATZKY

Materials Science Center, Department of Solid State and Applied Physics University of Groningen 9747 AG Groningen, The Netherlands

(Received September 25, 1990)

In this paper we study the valence electronic structure of $3d$ transition metal compounds in an Anderson impurity approximation. Using simplified models we arrive at a classification scheme (in terms of several parameters) for the nature of the band gaps in these materials. Mott-Hubbard insulators, in the simple sense, are special cases in this scheme. Another important class of insulators is characterized by light holes of ligand p character and heavy d-like electrons (charge-transfer semiconductors). Within the same theoretical basis we develop the theory describing the photoemission and inverse photoemission spectra from which one can obtain values for the parameters in the Anderson impurity Hamiltonian. Using an exact two particle Green's function formalism the photoemission of $CuCl_2$ is studied and it is shown that this compound is a charge-transfer semi-conductor. For the more general case an approximate, easy to use method is developed and is applied to the (inverse) photoemission of NiO. It is shown that NiO can be characterized as being intermediate between the Mott-Hubbard and charge-transfer regimes.

§ 1. Introduction

It is well established that the electronic structure of many $3d$ transition metal compounds (TMC's) cannot be described by standard band structure theory. This is most clearly evidenced by the presence of large conductivity gaps in many of these materials for which bandstructure theory predicts (nearly) metallic behaviour. Mott[1] and Hubbard[2] provided a basic solution to this problem by pointing out that an (effective) one electron description of solids is expected to break down if the Coulomb and exchange energies U involved in charge fluctuations of the type $d_i^n d_j^n \rightarrow d_i^{n-1} d_j^{n+1}$ (where i and j label sites and n the d orbital occupation) are large compared to the one electron dispersional width (W). For $U \gg W$ polarity fluctuations as above are surpressed and a correlation gap of order U is found in the excitation spectrum.

The Mott-Hubbard theory in its simplest form (i.e., taking into account only the TM d orbitals) is not sufficient to account for the bewildering variety of physical properties encountered in these compounds. According to the Mott-Hubbard theory the band gap is a d-d gap. However, it is known that at least for compounds of Ni, Co, Fe and Mn and the high T_c cuprates the gap scales with the ligand

*) Present address: AT&T Bell Laboratories, 600 Mountain Avenue, Murray Hill, NJ 07974-2070, U. S. A.

electronegativity which is indicative of a gap of the charge transfer type (ligand p-TM d).[4] It is also difficult to understand that many chalcogenides are metals[5] since this would require a reduction of U from 7~10 eV in the oxides[6),7)] to 1~2 eV in the sulfides. These observations all point at the importance of especially the ligand p-charge degrees of freedom, and the p-d covalency, with respect to the electronic properties of TMC's. The importance of ligand p states is manifest by the qualitative success of ligand field theory for the description of the low energy properties of these systems[3] such as the covalent reduction of the free ion Racah parameters as observed by optical spectroscopy and the spin delocalization as evidenced by transferred and supertransferred hyperfine fields. In ligand field theory it is the hybridization of the d-orbitals with (mainly) the ligand p orbitals which is of central importance.

In the past, a more detailed understanding of the nature of the bandgaps in these compounds has been hampered by the lack of clear experimental information concerning the energetics of the charge degrees of freedom. Central to the older work[8] are transport studies, but the interpretation of these measurements is severely hampered by the presence of many defects even in the most pure materials and the importance of electron lattice interactions (mobility) which obscure the view of the global electronic properties. Also the optical data could not be interpreted in an unambiguous way.[8),9)] A great improvement has come about with the advent of modern high energy spectroscopies (core-photoemission, Auger, X-ray absorption, (inverse) photoemission). With these spectroscopies the electronic degrees of freedom in the solid are directly probed and, moreover, they share a sensitivity to the correlated nature of the electrons. For instance, the understanding of such data in the field of mixed-valence materials, has played a key role in understanding their physical properties (for a recent review see Ref. 10)). Another example is the band narrowing

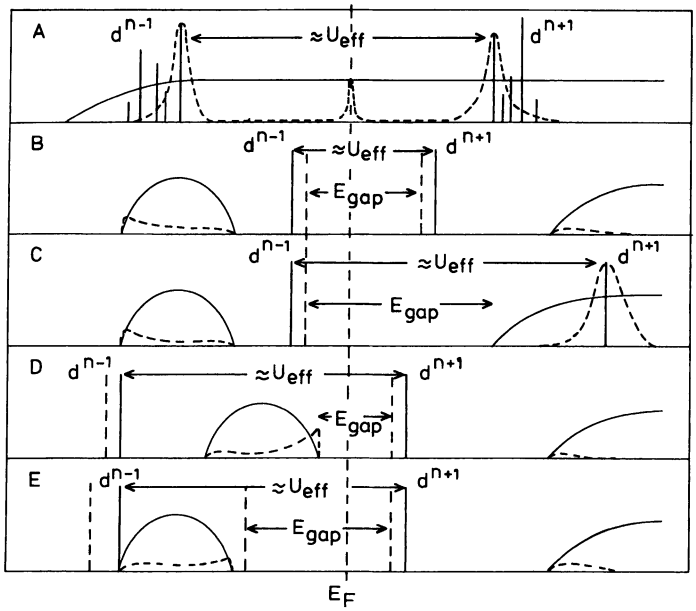

Fig. 1. An artist concept of the possible situations encountered for strongly correlated impurities in solids. Dashed lines indicate the effect of hybridization.

and two-hole satellite observed in the photoemission spectra of elemental Ni which illuminates the correlated nature of this material.[11] Recent interpretations of core level spectroscopies of transition metal compounds have also yielded important information concerning the valence electronic structure.[12),13)]

Perhaps the most direct probe of the valence electronic structure is the combination of valence-photoemission and inverse photoemission. If the post-collisional interaction between the emitted electron and the system left behind can be neglected (sudden approximation), which is usually assumed to be the case, this combination is precisely the Lehman spectral representation of the single electron Green's function convoluted with the optical matrix elements. In Fig. 1 we have sketched a zero-order picture of what can be expected for this quantity in the specific case of transition metal compounds.[14] In Fig. 1(A) we illustrate the well-established situation in mixed valence materials. In the ground state the correlated ions will have integral valence (d^n) if the mixing with the metallic band states is neglected. The addition or removal of a d-electron will lead to the multiplet split d^{n+1} and d^{n-1} manifolds. A measure for the strength of the Coulomb interaction between the d electrons is (IR_0 denotes the Hunds rule ground state irreducible representation)

$$U_{\text{eff}}=E(d^{n-1}, IR_0)+E(d^{n+1}, IR_0)-2E(d^n, IR_0)\,.$$

If this quantity is large, these manifolds will be well separated as indicated in the figure. The basic correctness of this picture for the rare earths is nicely demonstrated by Lang et al. in the (inverse) photoemission spectra.[15] Upon switching on the hybridization between the f-states and the band states the spectral line shape becomes complicated. The component (f^{n-1} and f^{n+1}) states broaden and shift and most important of all a sharp peak develops at E_F which is identified with the Kondo resonance. As Gunnarsson and Schönhammer showed, these line shapes for rare earth systems can be described in fair detail using the Anderson Impurity model.[16),17)]

In transition metal compounds a sowewhat similar situation is expected. Again we would expect the d^{n+1} and d^{n-1} manifolds to show up in the (inverse) photoemission. Moreover we have also to consider the non-d electronic degrees of freedom and with respect to these we can rely on band structure theory. Band structure calculations indicate that one usually has a relatively narrow ($\approx$4 eV) occupied ligand p band separated by a large gap from the unoccupied TM 4s like conduction band[18] (as shown in Fig. 1(B)). The d^n manifolds can now be positioned in different ways with respect to these bands, as indicated in Figs. 1(B)$\sim$(E). The direct relationship with the nature of the band gap is clear: The gap can be either of d-d (Mott-Hubbard, 1(A)), d-4s (1(C)) or p-d (1(D), 1(E)) character.

As in the case of mixed valence compounds the photoemission line shapes have, at first glance, not so much in common with this simple picture. It is however clear that the spectra cannot be interpreted in a one-particle framework. Satellites are seen in the spectra[19] and in ionic compounds it is possible to correlate the near threshold structures with the d^{n-1} multiplet structure.[20)~24)] The first attempt to interpret these spectra in a many-body framework is by Van der Laan et al.[25] who used a simple configuration interaction model of a small cluster, including p-d

hybridization, to interpret the photoemission spectrum of $CuCl_2$. More recently, Fujimori and Minami[26] showed that the results of a similar, although more extensive, calculation compare reasonably with the observed Nio and $NiCl_2$ photoemission line shapes. According to this calculation the lowest energy band in the photoemission spectrum of NiO is of strongly mixed O2p-Ni3d character. Subsequently, Sawatzky and Allen[6] and Hüfner et al.[7] recognized that the character of the lowest ionization- and affinity states as determined from the electron spectroscopies is intimately related to the nature of the conductivity gap. From the work of Fujimori and Minami together with the d-like signature of the lowest affinity states in the BIS spectrum, they concluded that the conductivity gap in NiO is not a Mott-Hubbard gap (d-d gap) but instead closer to a p-d (charge transfer) gap.

From the work of Fujimori and Minami[26] the important role of the p-d hybridization becomes clear. This hybridization is quite strong in the TMC's and to arrive at a sensible description of the (inverse) photoemission spectra and the bandgap it is necessary to take it fully into account. The multiplet splitting is quite large (≈ 8 eV) and should also be treated in full detail.[26] On the other hand, it is assumed in the cluster approach that the width's of the bands can be neglected. This is reasonable for the d-band because its dispersional width is quite small (≈ 0.5 eV) according to the bandstructure calculations.[18] However, the width of the ligand bands is relatively large (≈ 4 eV) and a bandstructure approach for these states is more realistic as confirmed by recent angular resolved measurements.[27)~29)]

In this paper we investigate the valence electronic structure of TMC's using a broken (translational) symmetry calculation for the TM-ions. This is equivalent to treating the d-states of the TM as impurity states in an anion lattice. Using impurity many-body theory[16),17)] it is then possible to give a full account of, on the one hand, the d-d Coulomb interactions including the atomic term splittings and, on the other hand, the p-d covalency and the itinearant nature of the 'host' valence and conduction bands. We showed previously that the core XPS and XAS[12] can be understood in this approach as well as the optical spectra and the superexchange.[30]

In § 2 we study the nature of the band gap using simplified models. We first consider a spin degenerate model and we obtain analytical expressions for the one electron Green's function using a two-hole Green's function technique[31] and an average T matrix method from Kanamori.[31] We point out the analogy with the Auger spectroscopy of filled impurities[32)~34)] and we arrive at a qualitative characterization of the band gap for situations where the conduction $4s$, p band can be neglected. Our findings are summarized in Fig. 1. If the d^{n-1} valence band separation is large compared to the hybridization (Fig. 1(D)) the gap will be of charge transfer character as indicated, irrespective of the ground state covalency. If the d^{n-1} state approaches the bottom of the valence band, a bound state will be pushed out of the valence band due to the p-d hybridization and the lowest ionization state is of strongly mixed p-d character (Fig. 1(E)). If the d^{n-1} state is further lowered we finally arrive at a Mott-Hubbard gap (Fig. 1(B)). Subsequently it is shown that the above picture also holds for the highly degenerate $3d$-ions[35] using numerical results obtained from a model in which multiplet effects are neglected.

In § 3 we show that the powerful two-hole Green's function techniques can be

generalized for highly degenerate impurities if the ground state can be approximated by a one-hole problem. Term splittings can be easily incorporated and the effect of these is discussed. This method applies to Cu(II) compounds and the high T_c cuprates.

Section 4 is aimed at the derivation of some controllable approximations which simplify the tedious calculations for many hole compounds. Using this method, the (inverse) photoemission spectrum of NiO is studied and it is concluded that this material is in between the Mott-Hubbard and change transfer regime.

§ 2. The systematics of band gaps

2.a. *Spin degenerate model*

In order to gain insight in the physics of a strongly correlated impurity in an insulating host it is instructive to consider a simple spin degenerate model. Assuming that the impurity states can be described with a tight binding orbital, the Hamiltonian is written as

$$\hat{H}=\hat{H}_0+\hat{H}_1\,,$$
$$\hat{H}_1=Un_{d\uparrow}n_{d\downarrow}\,. \tag{2·1}$$

$\hat{H}_1$ describes the Coulomb interaction between the impurity ('d') electrons) and $\hat{H}_0$ contains the one electron interactions which can be modelled by for instance the Anderson Impurity Hamiltonian[36]

$$\hat{H}_0=\sum_\sigma\Big[-\varepsilon_d n_{d\sigma}-\int_{-B}^{B}d\varepsilon(\varepsilon_L+\varepsilon)n_{\varepsilon\sigma}+\int_{E_c}^{\infty}dEEn_{E\sigma}$$
$$+\int_{-B}^{B}d\varepsilon V(\varepsilon)(d_\sigma{}^+c_{\varepsilon\sigma}+\text{h.c.})+\int_{E_c}^{\infty}dEV(E)(d_\sigma{}^+c_{E\sigma}+\text{h.c.})\Big]\,. \tag{2·2}$$

The first term in Eq. (2·2) describes the impurity orbital, the second term the host valence band with width $W=2B$ and the third term the host conduction band. The last two terms describe the hybridization between the impurity state and the valence- respectively conduction band states. The host states as appearing in Eq. (2·2) are projected in the impurity point group so that the k-labels have to be replaced by energy labels.[10),16)]

If U could be neglected (or taken into account in an average way) this problem would be solved by constructing single-particle eigenstates, in second quantization,

$$b_{i\sigma}^+=\alpha_i{}^*d_\sigma{}^++\int d\varepsilon\beta_i{}^*(\varepsilon)c_{\varepsilon\sigma}^+\int dE\gamma_i{}^*(E)c_{E\sigma}^+\,, \tag{2·3}$$

and the ground state would be given by

$$|\Phi_0\rangle=\prod_{i,\sigma}^{E_F}b_{i\sigma}^+|\text{vac}\rangle\,. \tag{2·4}$$

However, if U becomes large compared to the hybridization many more determinants like in Eq. (2·4) would be important in the ground state of the system. It is then

more practical to start with the eigenstates of the unhybridized problem as a zero order with the hybridization as the perturbation. For a half filled impurity shell we have the zero order ansatz

$$|d^1\rangle = d_\uparrow{}^+|\varphi'\rangle\,, \tag{2·5}$$

where $|\varphi'\rangle$ denotes the filled host valence band

$$|\varphi'\rangle = \prod_{\varepsilon\sigma} c^+_{\varepsilon\sigma}|\mathrm{vac}\rangle\,. \tag{2·6}$$

The state (2·5) couples to states like

$$|d^2\varepsilon\rangle = d_\uparrow{}^+ d_\downarrow{}^+ c_{\varepsilon\downarrow}|\varphi'\rangle\,, \tag{2·7}$$

where an electron has hopped from the valence band into the impurity shell and

$$|d^0 E\rangle = c^+_{E\uparrow}|\varphi'\rangle\,, \tag{2·8}$$

where the impurity electron has hopped into the conduction band. The states in Eqs. (2·7) and (2·8) are in turn coupled to states with a (conduction) electron-(valence) hole pair like

$$|d^1 E\varepsilon\rangle \propto d_\sigma{}^+ c^+_{E\sigma'} c_{\varepsilon\sigma''}|\varphi'\rangle\,. \tag{2·9}$$

These states are similar to the state we started with (Eq. (2·5)) except for the additional electron-hole pair and in principle we should continue this basis expansion to infinity. In metallic hosts the electron-hole pair can be placed at the Fermi-level with the consequence that the states in Eqs. (2·5) and (2·9) are degenerate. This leads to the infrared divergencies which makes the Kondo- and Mixed Valence problems difficult to handle.[16),17)] However, for a non-zero host gap these divergencies around the Fermi-level are removed and the states in Eq. (2·5) have a finite weight in the ground state wave function. In principle it is therefore possible to find the ground state wave function to any desired accuracy using this expansion.

Having the late $3d$-compounds in mind we can introduce a further simplification. It is well known that the valence band-$3d$ mixing is of much more importance than the conduction band-$3d$ mixing. The reason is that the on site $3d$-$4s$ mixing is at least in cubic point groups symmetry forbidden and the hybridization is therefore with the next nearest-neighbours. Furthermore, normally the bottom of the conduction band is relatively high lying in the late $3d$ compounds. It is therefore a sensible approximation to neglect the coupling to the conduction band states. In this case only a finite number of holes have to be treated. For instance, in order to obtain the ground state of a d^n impurity only $10-n=N$ holes have to be considered and a complete configuration interaction basis is given by all possible distributions of these holes among the host valence band and impurity states. In the same way the photoemission- and inverse photoemission spectra (and therefore the character of the bandgap) can be determined by considering $N+1$ and $N-1$ hole problems.

For the specific example of a spin-degenerate half-filled impurity these problems can be worked out analytically and the picture we obtain is in essence similar to that obtained for $3d$ impurities which will be investigated in detail in the next sections.

Considering the ground state of the half-filled impurity we notice that only a single, for instance spin-up, hole is present in the ground state. There are no other holes present to correlate with, so a single particle description will suffice for the ground state. We write

$$|\Psi_0\rangle = b_{0\uparrow}|\varphi\rangle . \tag{2·10}$$

Here $|\varphi\rangle$ represents the filled band system

$$|\varphi\rangle = d_\uparrow{}^+ d_\downarrow{}^+ |\varphi'\rangle \tag{2·11}$$

and

$$b_{i\sigma}^+ = \alpha_i{}^* d_{i\sigma}^+ + \int d\varepsilon \beta_i{}^*(\varepsilon) c_{\varepsilon\sigma}^+ , \tag{2·12}$$

where $b_{0\sigma}$ creates a hole in the highest occupied one-particle level. Using straightforward variational theory[18] we find for the ground state energy (with respect to $\langle\varphi|H|\varphi\rangle=0$)

$$E_0 = \varepsilon_d + \delta , \tag{2·13}$$

where δ is the hybridization shift determined from

$$\delta = \int_{-B}^{B} \frac{d\varepsilon |V(\varepsilon)|^2}{\delta - \Delta - \varepsilon} , \tag{2·14}$$

where $\Delta = \varepsilon_d + U\langle n_{d\downarrow}\rangle - \varepsilon_L$, $\langle n_{d\downarrow}\rangle = 1$ is the energy required to transfer the hole from the impurity to the centre of the ligand band which we call the charge-transfer energy. Also the d-hole count can be determined

$$\langle n_{d\uparrow}\rangle \equiv \langle n_d\rangle \equiv |\alpha_0|^2 = \left(1 + \int \frac{d\varepsilon |V(\varepsilon)|^2}{(\delta - \Delta - \varepsilon)^2}\right)^{-1/2} . \tag{2·15}$$

Having specified the nature of the ground state we now turn to the calculation of the d electron addition/removal spectra as seen in (inverse) photoemission spectra. The inverse photoemission spectrum is in the sudden approximation given by

$$\rho_d{}^>(\omega) = \frac{1}{\pi}\sum_\sigma \mathrm{Im} G_{d\sigma}^>(\omega - i0^+) ,$$

$$G_{d\sigma}^>(z) = \langle \Psi_0 | d_\sigma \frac{1}{Z - H + E_0} d_\sigma{}^+ | \Psi_0\rangle , \tag{2·16}$$

where we only consider the filling of the d-states. It is evident that only the completely filled state in Eq. (2·11) can be reached by adding an electron. In the absence of U it is essential that $\varepsilon_d + \delta = 0$ in order to have Eq. (2·10) as the ground state. In the correlated case this will turn out to be an arbitrary choice for the Fermi energy. Using this convention we find a single line in the BIS spectrum with weight $\langle n_d\rangle$ at zero energy

$$\rho_d{}^>(\omega) = \langle n_d\rangle \delta(\omega) . \tag{2·17}$$

The photoemission spectrum (assuming only d-emission) is given in the sudden

approximation by

$$\rho_d{}^<(\omega)=\frac{1}{\pi}\sum_\sigma \mathrm{Im}G^<_{d\sigma}(\omega-i0^+)\,,$$

$$G^<_{d\sigma}=\langle\Psi_0|d_\sigma{}^+\hat{G}d_\sigma|\Psi_0\rangle\,,$$

$$\hat{G}=(z+\hat{H}-E_0)^{-1}\,. \tag{2·18}$$

Upon removing an electron from the ground state things are not trivial because now two holes are present which are correlated for non-zero U. In order to calculate the spectrum we treat the d-d Coulomb interaction (H_1) as the perturbation and we write

$$\hat{G}=\hat{G}_0+\hat{G}_0\hat{T}\hat{G}_0\,, \tag{2·19a}$$

$$\hat{T}=\hat{H}_1+\hat{H}_1\hat{G}_0\hat{T} \tag{2·19b}$$

with

$$\hat{G}_0=(z+\hat{H}_0-E_0)^{-1}\,. \tag{2·20}$$

Combining Eqs. (2·18) and (2·19a) we find for the spin down emission

$$G^<_{d\downarrow}=\langle\Psi_0|d_\downarrow{}^+\hat{G}_0d_\downarrow|\Psi_0\rangle+\langle\Psi_0|d_\downarrow{}^+\hat{G}_0\hat{T}\hat{G}_0d_\downarrow|\Psi_0\rangle\,. \tag{2·21}$$

In order to evaluate Eq. (2·21) we introduce the uncorrelated two-hole basis

$$|\varphi_{ij}\rangle=b_{i\downarrow}b_{j\uparrow}|\varphi\rangle\,. \tag{2·22}$$

We have the useful equalities

$$\langle\varphi_{i0}|\hat{G}_0|\varphi_{jk}\rangle=\delta_{ij}\delta_{0k}g_i(z) \tag{2·23}$$

with

$$g_i(z)=\frac{1}{z+E_i-E_0}\,,$$

$$E_i=\langle\varphi|b^+_{i\sigma}\hat{H}_0b_{i\sigma}|\varphi\rangle \tag{2·24}$$

and

$$\langle\Psi_0|d_\downarrow{}^+|\varphi_{i0}\rangle=\alpha_i\,. \tag{2·25}$$

Equation (2·21) can be expanded using the identity operator $1=\sum_{ij}|\varphi_{ij}\rangle\langle\varphi_{ij}|$ and together with Eqs. (2·23)~(2·25) we find

$$G^<_{d\downarrow}(z)=\sum_i|\alpha_i|^2g_i(z)+\sum_{ij}\alpha_i{}^*g_i(z)\langle\varphi_{i0}|\hat{T}|\varphi_{j0}\rangle\cdot g_j(z)\alpha_j\,. \tag{2·26}$$

The matrix elements of T are zero except

$$T^{dd}_{dd}=\langle\varphi|d_\uparrow{}^+d_\downarrow{}^+\hat{T}d_\downarrow d_\uparrow|\varphi\rangle=U+Ug^{dd}_{dd}(z)T^{dd}_{dd} \tag{2·27}$$

with

$$g^{dd}_{dd}(z)\equiv\langle\varphi|d_\uparrow{}^+d_\downarrow{}^+\hat{G}_0d_\downarrow d_\uparrow|\varphi\rangle\,, \tag{2·28}$$

and we find

$$T_{dd}^{dd}=\frac{U}{1-Ug_{dd}^{dd}(z)}\,. \tag{2·29}$$

From Eqs. (2·27) and (2·22) it follows that

$$\langle\varphi_{i0}|\hat{T}|\varphi_{j0}\rangle=|\alpha_0|^2\alpha_i\alpha_j{}^*T_{dd}\,. \tag{2·30}$$

Combining Eqs. (2·26), (2·29) and (2·30) we finally arrive at

$$G_{d\downarrow}^{<}(z)=g_d{}^d(z)+g_d{}^d(z)\langle n_d\rangle\frac{U}{1-Ug_{dd}^{dd}(z)}g_d{}^d(z)\,, \tag{2·31}$$

where we defined

$$g_d{}^d(z)=\sum_i|\alpha_i|^2g_i(z)\,. \tag{2·32}$$

Considering Eq. (2·31) we first notice that $g_d{}^d$ is the usual one-particle impurity Green's function as would follow from a (mean-field) calculation of the neutral state of the system. Alternatively we can write

$$g_d{}^d(z)=\int_{-\infty}^{\infty}\frac{\rho_d(\omega)d\omega}{z-\omega}\,, \tag{2·33}$$

where $\rho_d(\omega)$ is the single-hole partial d density of states. We see that for zero U the non-interacting limit is reproduced. Because the lowest pole of Eq. (2·33) coincides in energy with the ground state no energy gap is present in this case.

For non-zero U however, the imaginary parts of Eq. (2·31) would be determined by the poles and branch-cuts of the T-matrix Eq. (2·29). A close analogy can now be drawn with the Auger spectroscopy of filled d-band metals[32] and impurities.[33),34] The photoemission spectra of these materials are usually quite well described by band structure theory. For instance, in the angular resolved photoemission spectra of the noble metals sharp peaks are seen which show a strong angular dependence indicating the bare hole $\underline{k}$ is a good quantum number. A satisfactory agreement is found with the dispersion curves obtained from local density theory.[37] In Auger spectroscopy it is basically the local two-hole density of states which is measured. In the one-particle picture one should expect to find the self-convolution of the one-hole density of states but instead one finds experimentally a spectrum which resembles the Auger spectrum of the free atom.[38]

An explanation is offered by the theory of Cini and Sawatzky.[32] In its simplest formulation one considers an impurity Hamiltonian like in Eq. (2·1). The Auger spectrum is given by

$$\rho_{dd}(\omega)=\frac{1}{\pi}\mathrm{Im}G_{dd}^{dd}(\omega-i0^+)\,, \tag{2·34}$$

where

$$G_{dd}^{dd}(z)=\langle\varphi|d_\uparrow{}^+d_\downarrow{}^+\frac{1}{z-H}d_\downarrow{}^+d_\uparrow{}^+|\varphi\rangle \tag{2·35}$$

is the two-hole Green's function. Along the same lines as in Eq. (2·29) it is easily shown that

$$G^{dd}_{dd}(z)=\frac{g^{dd}_{dd}(z)}{1-Ug^{dd}_{dd}(z)}\,. \tag{2·36}$$

We can write $g^{dd}_{dd}(z)$ (Eq. (2·28)) as the self-convolution of the one-hole Green's functions

$$g^{dd}_{dd}(z)=\frac{1}{2\pi i}\int_{-\infty}^{\infty}d\xi g^{d}_{d}(\omega-\xi)g_{d}{}^{d}(\xi)\,, \tag{2·37}$$

and it is found that for $U\gg W$ the imaginary part of Eq. (2·36) is dominated by a pole at $\approx U$ corresponding with a state where both holes are localized on the same site, which explains the atomic signature of the spectrum.

The parallel with our case may be clear. The ground state of the filled impurity corresponds with the state reached by adding an electron to the half-filled impurity. The states reached in the Auger process of the filled impurity and the photoemission of the half-filled impurity are the same although the intensity distribution in these spectra is different because of the different initial states involved, as is reflected in the differences between Eqs. (2·31) and (2·36).

In order to discuss the physical content of Eq. (2·31) we can roughly follow the analysis given by Drchall and Kudrnovsky and others[32)~34)] of the Auger spectra. We

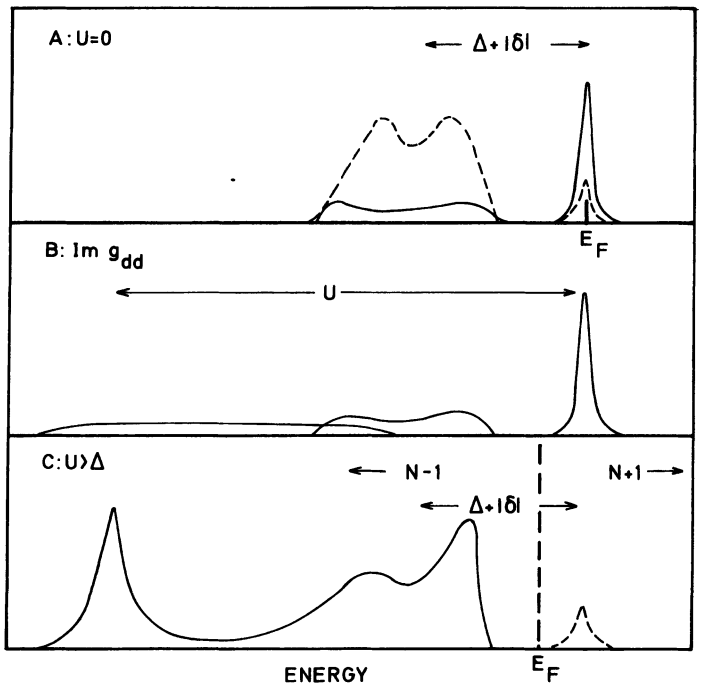

Fig. 2. States and continua as found in the calculation of the photoemission of the spin-degenerate impurity. In Fig. 1(A) the one-hole impurity D. O. S. is indicated together with the peak in the BIS spectrum and the host density of states (dashed lines). In Fig. 1(B) we show the different contributions to the uncorrelated two-hole density of states and in Fig. 1(C) we show an artist's impression of the (inverse) photoemission spectrum for U as indicated.

are interested in the situation where in the one-particle picture the d-band is located at E_F and the ligand band lies considerably below E_F. We write the one-hole impurity Green's function as

$$g_d^d(z)=\frac{\langle n_d\rangle}{z}+R(z)\,, \tag{2·38}$$

which is composed of a pole at $E_F=0$ with weight $\langle n_d\rangle$ and a regular part $R(z)$ corresponding to the d-character mixed into the host valence band (see Fig. 2(A)). Inserting Eq. (2·38) in Eq. (2·37) we find

$$g_{dd}^{dd}(z)=\frac{\langle n_d\rangle^2}{z}+2\langle n_d\rangle R(z)+S(z)\,, \tag{2·39}$$

where

$$S(z)=\frac{1}{2\pi i}\int_{-\infty}^{\infty}R(z-\xi)R(\xi)d\xi\,. \tag{2·40}$$

The three terms in Eq. (2·39) give three different types of the states of a pair of holes with opposite spin for $U=0$. The first term corresponds to a localized state with both holes in the bound one-particle state (see Fig. 2(B)). The second term gives mixed states where one hole is in the ligand band while the other is localized and the third term corresponds to states where both holes are in the ligand band. These three terms characterize the Auger spectrum for the filled impurity for $U=0$. In our case the ground state hole would be bound to the impurity while the second hole created in the photoemission process would either also be bound or in the ligand band in the non-interacting limit.

For $U>0$ the zero energy pole in the photoemission spectrum vanishes (as in the Auger spectrum). For $z\to 0$, $g_d^d\to\langle n_d\rangle/z$, $g_{dd}^{dd}(z)\to\langle n_d\rangle^2/z$ and we find from Eq. (2·31) that $G_d^<(z)$ is real for $z\to 0$

$$\lim_{z\to 0}G_d^<(z)=\frac{(U(\langle n_d\rangle R(z)+S(z))-1)}{U\langle n_d\rangle}\,. \tag{2·41}$$

As a result, a gap appears between the affinity state $|\varphi\rangle$ and the lowest ionization state with the Fermi-energy somewhere in this gap, and an insulator is predicted.

New poles will be found if the denominator of the T-matrix vanishes, that is under the conditions

$$\mathrm{Re}\,g_{dd}^{dd}(E_B)=\frac{1}{U}\,,\qquad \mathrm{Im}\,g_{dd}^{dd}(E_B)=0\,. \tag{2·42}$$

Besides these bound states, spectral weight will also be found in the regions where $R(z)$ of $S(z)$ have a non-zero imaginary part, corresponding with band-like holes. Considering the limit $U\gg\Delta+|\delta|$, $R(z)\to(1-\langle n_d\rangle)/z$ and $S(z)\to(1-\langle n_d\rangle)^2/z$ and a pole results in $G^<$ for $z=U$ with weight $\langle n_d\rangle$. In the ionic limit ($\langle n_d\rangle=1$) we therefore find the 'atomic' spectrum with a 'd^2' line in the BIS spectrum and a 'd_0' line in the photoemission separated by U. On the other hand, if the ground state is to some extent covalent, only a fraction $\langle n_d\rangle$ of the total intensity goes into the two-hole

satellite and the remainder $(1-\langle n_d\rangle)$ goes into the bands (see Fig. 2(C)).

It will be clear that in this limit no pole can be found above the top of the $R(z)$ band, at least if the valence band density of states is continuous. This implies that the lowest electron removal states correspond with states where one hole is bound to the impurity (in the same way as in the ground state) while the other hole moves freely in the host valence band. According to the parametrization used in Eqs. (2·13) and (2·14) the splitting between the top of the $R(z)$ band and the affinity peak, which is the band gap in this regime, equals $\Delta+|\delta|-\frac{1}{2}W$ (see Fig. 2(C)). This is the energy required to move a hole from the cation to the anion and therefore we called this gap a charge-transfer gap.[35]

This implies for the concentrated limit that the electrons are moving in a narrow Hubbard-like band with a width (according to canonical perturbation theory[39]) $w_e \propto V^2/\Delta$. On the other hand, the holes move in the broad host valence band and will experience only an exchange interaction with the spins of the holes localized on the cations. It is this large difference between the electron- and hole effective mass which is the outstanding property of these class of materials. We notice that this picture holds, in principal, rather independently of the degree of covalency. Also for non-integral valence the charge-degrees of freedom of the hole localized on the impurity are projected out so that the difference between 'Kondo'- and 'Mixed-valence' regimes as is relevant to metals does not apply to the insulators.

Returning to the model, upon decreasing U for fixed Δ at a certain point condition Eq. (2·41) will be fulfilled in the region above the host valence band maximum and a bound state will be pushed out of the $R(z)$ band. This state will correspond with a hole which is still quite delocalized due to the strong admixing of the ligand band states. At the same time it has the symmetry properties of the singly ionized bare impurity which will become more evident in §§ 3~5. There we consider $3d$-impurities and we show that the multiplet spectrum of the bare $3d^{n-1}$ impurity is to some extent reflected in the gap region of the host.

Upon further decreasing U we enter a point where U is smaller than the charge transfer gap. In this regime the gap magnitude scales with U and the Mott-Hubbard theory becomes a better starting point for the study of the low lying electronic excitations. As is evident, the holes and electrons will now move in bands of roughly similar width (according to the canonical perturbation theory) $w_e \propto V^2/\Delta$, $w_h = V^2/|\Delta-U|$.

2.b. *Highly degenerate model*

In order to show that this picture of the band gap systematics also applies to the highly degenerate $3d$-impurities we finish this section with a model calculation which applies more directly to the late $3d$-compounds. The generalization of Eq. (2·1) for a $3d$-impurity reads[10] (under the neglect of the conduction band)

$$H = H^{\text{host}} + H^{\text{imp}} + H^{\text{hybr}},$$

$$H^{\text{host}} = -\sum_m \int d\varepsilon(\varepsilon-\varepsilon_L) c^+_{\varepsilon m} c_{\varepsilon m},$$

$$H^{\text{imp}}=-\sum_m \varepsilon_{dm} d_m{}^+ d_m + \sum_{ijlm} U(ijlm) d_i{}^+ d_j d_l{}^+ d_m \,,$$

$$H^{\text{hybr}}=\sum_m \int d\varepsilon\, V_m(\varepsilon)(d_m{}^+ c_{\varepsilon m} + c_{\varepsilon m}^+ d_m) \,. \tag{2·43}$$

Compared to Eq. (2·1), in Eq. (2·2) the summation m now includes besides of σ also the m_l quantum numbers. Further, the d-shell can be split in subshells because of the crystal field interactions (e_g and t_{2g} in the usual O_h symmetry). Finally, the d-d interactions are not only described by the monopole term (F_0) but also by the higher order interactions which give rise to multiplet splitting.

In order to have a tractable model which at the same time applies to Mn, Fe, Co and Ni compounds we introduce some simplifications. First, it is well known that the π-like transfer integrals are considerably smaller than the σ-like transfer integrals which allows us to neglect the former. In O_h symmetry this means that the hybridization of the t_{2g} states is neglected and we assume that the t_{2g} holes, if present, can be considered as spectator holes. Second, we neglect the multiplet effects arising from the exchange and multipole d-d Coulomb interactions. These effects will be treated extensively in the next sections. Under these assumptions the calculation of the gap of high spin Ni to Mn compounds involves a two e_g-hole problem for the ground state, a single e_g-hole affinity problem and a three e_g-hole electron removal problem. Unfortunately, it is not possible to extend the two-hole Green's function approach to a three-hole problem (at least no closed solutions are found). An alternative is then the approach where we expand the problem in a Hilbert space spanned by all ionic configurations with the hybridization as the perturbation.

As a reference state we take

$$|d^{n+2}\rangle = \prod_{m\in t_{2g}} d_m{}^+ \prod_{m\in e_g=1}^{4} d_m{}^+ \prod_{\varepsilon m} c_{\varepsilon m}^+ |\text{vac}\rangle \,, \tag{2·44}$$

where the e_g- and host valence band are completely filled while we allow for a partly filled t_{2g} band. A filled t_{2g} band would correspond with a Ni-compound and a half-filled t_{2g} band with a Mn-compound. For the ground state we take the zero order ansatz

$$|d^n\rangle = d_1 d_2 |d^{n+2}\rangle \,, \tag{2·45}$$

where the symmetry labels now refer to $1=d_{x^2-y^2}$ and $2=d_{3z^2-r^2}$. This state couples to

$$|d^{n+1}\varepsilon\rangle = \frac{1}{\sqrt{2}}(d_1 c_{\varepsilon 2} + c_{\varepsilon 1} d_2)|d^{n+2}\rangle \,, \tag{2·46}$$

where we combined degenerate states as in $1/N$ theory which gives the non-diagonal matrix elements

$$\langle d^n|H|d^{n+1}\varepsilon\rangle = \sqrt{2}\, V(\varepsilon) \,. \tag{2·47}$$

The states in Eq. (2·46) couple in turn to states where both e_g-holes are delocalized in the valence band. In the same way we can find the basis for the electron

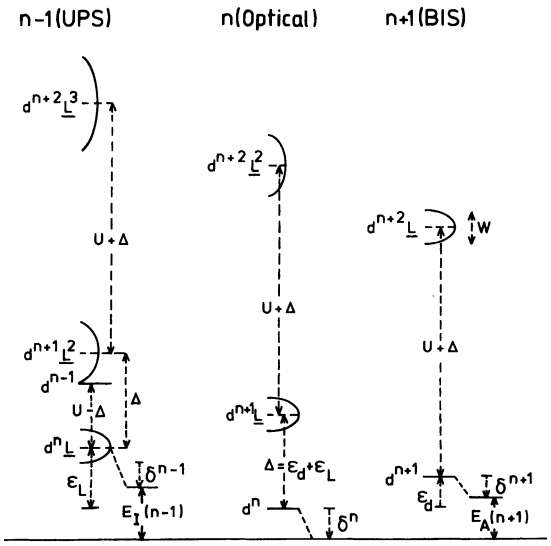

Fig. 3. Total energy diagram indicating the states and continua entering the model calculation as described in the text. Hybridization shifts are also indicated.

addition and the electron removal states. In the latter case we use the zero order ansatz

$$|d^{n-1}\rangle = d_1 d_2 d_3 |d^{n+2}\rangle\,, \qquad (2\cdot48)$$

where d_3 corresponds with a spin down hole in either the $d_{x^2-y^2}$ or $d_{3z^2-r^2}$ orbital. A survey of all the basis states and matrix elements can be found in Appendix A and these findings are summarized in a total energy diagram (Fig. 3). We have parametrized the diagonal matrix as follows: With respect to $\langle d^n|H|d^n\rangle \equiv 0$ it costs ε_d to create a d electron and ε_L to create a ligand hole such that $\Delta = \varepsilon_d + \varepsilon_L$ is the charge tranfer energy. Moreover, with this definition of ε_d the d^{n-1} state is located at $-\varepsilon_d + U$ and the d^{n+2} state at $2\varepsilon_d + U$. The other matrix elements follow easily.

It is not possible to find analytical solutions using this expansion (except for the trivial one-hole problem) as discussed by Gunnarsson and Schönhammer.[16] Instead, we discretize the valence band in N_ε (equidistant) states using as a model density of states

$$|V(\varepsilon)|^2 = V^2 \frac{2}{\pi B^2}(\varepsilon^2 + B^2)^{1/2}\,; \quad -B \le \varepsilon \le B\,. \qquad (2\cdot49)$$

The ground states of the resulting three large eigenvalue problems can be found by using the efficient Chebyshev-polynomial method.[17]

In Fig. 4 we show results obtained with $N_\varepsilon = 40$ for the band gap magnitudes, obtained from

$$E_{\text{gap}} = E_0(N+1) + E_0(N-1) - 2E_0(N)\,, \qquad (2\cdot50)$$

where $E_0(N+1)$, $E_0(N-1)$ and $E_0(N)$ are the ground state energies of respectively the electron addition, electron removal and neutral states of the system. These are derived for different U, Δ and W in units of V. Further we show the average charge of e_g symmetry present on the transition metal ion in these ground states as a function of the same parameters.

First we notice that for $U=0$ always a zero band gap is found and the d-counts follow statistical rules ($\langle n_d\rangle^N = 2\langle n_d\rangle^{N-1}$, $\langle n_d\rangle^{N+1} = 3\langle n_d\rangle^{N-1}$), as in one electron theory. This is a difficult limit and these results show the accuracy of the calculation (a total of 12341 configurations are involved in the $N-1$ calculation).

For non-zero U these results reaffirm the qualitative picture of the previous section. For $\Delta \gg U$ the gap is proportional to U, corresponding with the Mott-

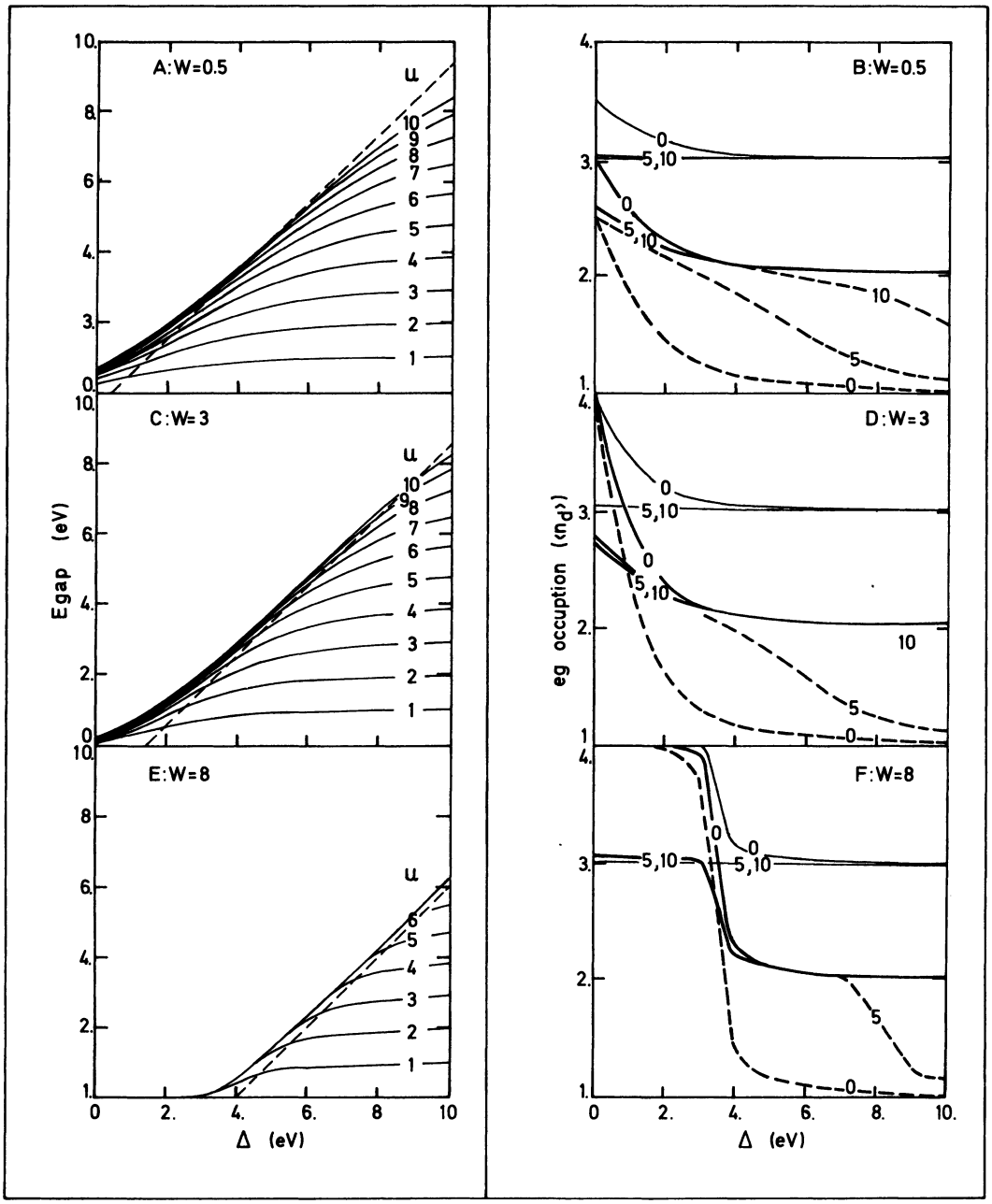

Fig. 4. Results of the band gap magnitudes as a function of Δ for various values of U (in eV) and bandwidth (W, in eV) ((A), (C), (E)). Dashed lines indicate $E_{gap}=\Delta-W/2$. In (B), (D) and (F) the e_g-occupations of the cations in the various states are indicated: Heavy lines correspond with $\langle n_d\rangle^N$, thin line with $\langle n_d\rangle^{N+1}$ and dashed line with $\langle n_d\rangle^{N-1}$. These are calculated for $U=0$, 5, 10 eV and the same bandwidths as in (A), (C) and (E).

Hubbard insulators. We write in this regime

$$E_{\text{gap}}=U+\delta^{N+1}+\delta^{N-1}-2\delta^{N}\,, \tag{2·51}$$

where δ^N, δ^{N+1} and δ^{N-1} are the hybridization shifts measured from respectively the $|d^N\rangle$, $|d^{N+1}\rangle$ and $|d^{N-1}\rangle$ basis state energies. For Δ large compared to both V^2, U and W bound state perturbation theory can be applied and it is found that

$$\begin{aligned} E_{\text{gap}} &\approx U+\frac{3V^2}{\Delta-U}+\frac{V^2}{\Delta+U}-\frac{4V^2}{\Delta} \\ &\approx U-\frac{2V^2}{\Delta}\left(\frac{U}{\Delta}\right), \end{aligned} \tag{2·52}$$

which indicates that the gap is always somewhat less than U because of the covalency.

On the other hand, for $\Delta<U$ the band gap magnitude is roughly proportional to $\Delta-(1/2)W$. Considering the charge distribution it is seen that in this regime $\langle n_d\rangle^{N-1}=\langle n_d\rangle^{N}$ showing that the additional hole created in the ionized state is fully delocalized in the host valence band. It turns out that (δ^N, δ^{N-1} both measured as indicated in Fig. 3)

$$E_{\text{gap}}=\Delta-\frac{1}{2}W+|\delta^{N}|\,, \tag{2·53}$$

and we called this in the last section a charge-transfer gap. Finally, we find a continuous cross over regime between the Mott-Hubbard and charge-transfer regions, where a bound state is pushed out of the ligand band due to the interaction with the $|d^{n-1}\rangle$ state.

It would be expected from Eq. (2·53) that the gap closes for $\Delta+|\delta^N|\approx(1/2)W$. This indeed happens according to our calculations which is interesting because it shows that a metal-to-insulator transition can be driven by a mechanism unrelated to the Mott-Hubbard mechanism. For instance, the charge transfer energy (Δ) decreases for decreasing anion electro-negativity and an insulator to metal transition is expected as a function of ligand electro-negativity. This explains for instance why the sulfides are usually metallic and the oxides insulators.[5]

Although we do not believe that this insulator calculation is suited to discuss the nature of the metallic state in detail it at least tells us why the transition occurs. As can be seen from Fig. 4(F) the ground state has changed its nature in the metallic regime. For large U the local hole count $\langle n_d\rangle^N=N+1$ which implies that one hole is now delocalized in the ligand band. In the concentrated case this implies that the Fermi-level is located within the ligand band. This category of materials is commonly called p-type metals and well-known examples are CuS.[40] Also the semiconducting pyrites are in this class where the ligand holes drive a Peierls like transition resulting in the formation of sulfur pairs.[41]

§ 3. (Inverse) Photoemission of one-hole compounds

As we showed before,[14] it is possible to calculate the (inverse) photoemission spectra using the scheme described in the previous section. However, these results compare rather poorly with experiment which is caused by the neglect of multiplet-splittings. The typical spread of multiplet energies, relevant to photoemission, is of the order of 5 eV and it is clear that these effects have to be taken into account explicitly. Upon inclusion of the multiplet effects the calculations become quite tedious and we will present in the next section a reasonably accurate and easy to handle approximate method which can be applied to a wide range of compounds. However, in the case where the ground state can be approximated by a single hole in a filled band it is again possible to use the two-hole Green's function technique of § 2.a, generalized for the highly degenerate case. In this section we will work this out in detail and apply it to the valence photoemission spectra of Cu(II) compounds.

In analogy with Eqs. (2·10)~(2·12) we write for the ground state of the one-hole impurity in the highly degenerate case

$$|\varphi_0;\Gamma\rangle=b_{0\gamma}|\varphi\rangle\,, \tag{3·1}$$

where Γ represents the ground state irreducible representation of the point group and

$$|\varphi\rangle=\prod_{im} b_{im}^{+}|\mathrm{vac}\rangle \tag{3·2}$$

represents the state of the system in which both the ligand band and the d-shell of the impurity are filled. The single particle operators are written as

$$b_{im}^{+}=a_i^{*}(m)d_m^{+}+\int d\varepsilon\beta_{im}^{*}(\varepsilon)c_{\varepsilon m}^{+}\,, \tag{3·3}$$

and $b_{0\gamma}$ creates a hole in the highest occupied orbital, with symmetry γ (for instance, in D_{4h}, $\Gamma={}^2B_1$ and $\gamma=b_{1\uparrow}$).

The photoemission current is, in the sudden approximation given by

$$\rho_{\mathrm{tot}}^{<}(\omega)\propto\frac{1}{\pi}\sum_{mm'\neq\gamma}\mathrm{Im}G_{\mathrm{tot}}^{<}(\gamma mm',\,\omega-i0^{+}) \tag{3·4}$$

with

$$G_{\mathrm{tot}}^{<}(\gamma mm',z)=\langle\Phi_0;\Gamma|\hat{A}_m^{+}(k_F)\hat{G}\hat{A}_{m'}(k_F)|\Phi_0;\Gamma\rangle\,, \tag{3·5}$$

where $\hat{G}=(z+\hat{H}-E_0)^{-1}$, $\hat{H}$ given by (2·43) and

$$\hat{A}_m(k_F)=\int d\varepsilon A_L(k_F,\varepsilon)c_{\varepsilon m}+A_d(k_F)d_m \tag{3·6}$$

with the transition matrix elements

$$\begin{aligned}A_d(k_F)&=\langle\Psi_{k_F}|\underline{A}\cdot\underline{p}|\Psi_{dm}\rangle\,,\\ A_L(k_F,\varepsilon)&=\langle\Psi_{k_F}|\underline{A}\cdot\underline{p}|\Psi_{\varepsilon m}\rangle\,,\end{aligned} \tag{3·7}$$

where $|\psi_{k_F}\rangle$, $|\psi_{dm}\rangle$ and $|\psi_{em}\rangle$ denote respectively the wave function of the emitted electron, the impurity- and host orbitals. For simplicity we neglected the m_1-dependence of the photoemission amplitudes.

Focussing first on d-emission only ($A_L=0$) we consider the Green's function

$$G^<_{dd}(\gamma mm', z)=\langle \Phi_0; \Gamma | d_m^+ \hat{G} d_{m'} | \Phi_0; \Gamma \rangle , \tag{3·8}$$

and this can be evaluated in a similar way to Eq. (2·18). We first write Eq. (3·8) in the T-matrix form and the resulting expression is evaluated using the uncorrelated two-hole basis

$$|\Phi_{ij}(mm')\rangle = b_{im} b_{jm'} |\Phi\rangle , \tag{3·9}$$

and we find

$$G^<_{dd}(\gamma mm', z)=g_d^d(m, z)\delta_{mm'}+g_d^d(m, z)\langle n_d\rangle T^{\gamma mm'}_{\gamma m} \cdot g_d^d(m', z) , \tag{3·10}$$

where $\langle n_d\rangle=|a_0(\gamma)|^2$ is the hole count on the impurity and ($E_{im}=\langle\varphi|b_{im}^+ \hat{H}_0 b_{im}|\varphi\rangle$)

$$g_d^d(m, z)=\sum_i \frac{|a_i(m)|^2}{z+E_{im}-E_0}=\int_{-\infty}^{\infty}\frac{\rho_d(m, \omega)d\omega}{z-\omega} \tag{3·11}$$

are the single-hole Green's functions, related to the single-hole partial d-densities of states ($\rho_d(m, \omega)$). In order to simplify the evaluation of the T matrix ($T^{m''m'''}_{mm'}=\langle\varphi|d_m^+ d_{m'}^+ \hat{T} d_{m''} d_{m'''}|\varphi\rangle$) it is convenient to project Eq. (3·10) on the two-hole irreducible representations of the point group (Γ_I)

$$G^<_{dd}(\gamma mm', z)=\sum_{\Gamma_I}\langle \gamma m|\}\Gamma_I\rangle\langle\Gamma_I|\}\gamma m'\rangle \cdot G^<_{dd}(\gamma mm', z; \Gamma_I) ,$$

$$G^<_{dd}(\gamma mm', z; \Gamma_I)=g_d^d(m, z)\delta_{mm'}+g_d^d(m, z)\, T^{\gamma mm'}_{\gamma m}(\Gamma_I) g_d^d(m', z) . \tag{3·12}$$

In Eq. (3·12) $\langle \gamma m|\}\Gamma_I\rangle$ is a short hand for the coefficients of fractional parentage

Table I. Electrostatic matrices of d^8 in D_{4h}.

$^3A_2$	b_1b_2	e^2
b_1b_2	$A+4B$	$6B$
e^2	$6B$	$A-5B$

$^1B_1$	a_1b_1	e^2
a_1b_1	$A+2C$	$-2B\sqrt{3}$
e^2	$-2B\sqrt{3}$	$A+B+2C$

^3E	eb_1	ea_1	eb_2
eb_1	$A-5B$	$-3B\sqrt{3}$	$3B$
ea_1	$-3B\sqrt{3}$	$A+B$	$-3B\sqrt{3}$
eb_2	$3B$	$-3B\sqrt{3}$	$A-5B$

^1E	eb_1	ea_1	eb_2
eb_1	$A+B+2C$	$-B\sqrt{3}$	$-3B$
ea_1	$-B\sqrt{3}$	$A+3B+2C$	$-B\sqrt{3}$
eb_2	$-3B$	$-B\sqrt{3}$	$A+B+2C$

$^1A_1$	a_1^2	b_1^2	b_2^2	e^2
a_1^2	$A+4B+3C$	$4B+C$	$4B+C$	$(B+C)\sqrt{2}$
b_1^2	$4B+C$	$A+4B+3C$	C	$(3B+C)\sqrt{2}$
b_2^2	$4B+C$	C	$A+4B+3C$	$(3B+C)\sqrt{2}$
e^2	$(B+C)\sqrt{2}$	$(3B+C)\sqrt{2}$	$(3B+C)\sqrt{2}$	$A+7B+4C$

a_1b_1 $^3B_1=A-8B$

b_1b_2 $^1A_2=A+4B+2C$

$\langle d(\gamma)d'(m)|\}\gamma m;\ \Gamma_I\rangle$. The matrix elements of the T matrix can be found by solving the system of linear equations

$$T_{\gamma m}^{\gamma m'''}(\Gamma_I)=H_{1\gamma m}^{\gamma m''}(\Gamma_I)+\sum_{m'm''}H_{1\gamma m}^{m'm''}(\Gamma_I)g_{m'm''}^{m'm''}(z)\,T_{m'm''}^{\gamma m'''}(\Gamma_I)\,, \tag{3·13}$$

where $H_{1\gamma m}^{m'm''}(\Gamma_I)$ are the matrix elements of the electrostatic d-d Coulomb matrices. These are given together with the coefficients of fractional parentage, in Table I for the I. R.'s of the point group D_{4h} (42). The uncorrelated two-hole Green's functions are obtained by convoluting the single-hole Green's functions

$$g_{m'm''}^{m'm''}(z)=\frac{1}{2\pi i}\int_{-\infty}^{\infty}g_d^{\,d}(m',\,z-\xi)g_d^{\,d}(m'',\,\xi)d\xi\,. \tag{3·14}$$

In order to calculate the photoemission spectra we need, aside from the electrostatic matrices of Table I, only the one-hole Green's functions. As we argued in § 2 it would make sense to use first principle band structure information for these. Here we will present results obtained by using the Anderson Impurity Hamiltonian to model the single particle interactions. The Cu(II) ions are usually in a square planar environment and the appropriate point group is D_{4h}. In this symmetry the d-shell is split into b_1, a_2, b_2 and e (all gerade) single-hole states and the ground state is of b_1 character. We model the one-hole Green's functions as

$$\begin{aligned}
&g_d^{\,d}(b_1\sigma,\,z)=(z-\delta-V_e^{\,2}\Gamma(z-\delta+\Delta))^{-1}\,,\\
&g_d^{\,d}(a_1\sigma,\,z)=(z-\delta+4Ds+5Dt-V_e^{\,2}\Gamma(z-\delta+\Delta))^{-1}\,,\\
&g_d^{\,d}(b_2\sigma,\,z)=(z-\delta+10Dq-V_t^{\,2}\Gamma(z-\delta+\Delta))^{-1}\,,\\
&g_d^{\,d}(e\sigma,\,z)=(z-\delta+10Dq+3Ds-5Dt-V_t^{\,2}\Gamma(z-\delta+\Delta))^{-1}
\end{aligned} \tag{3·15}$$

with

$$\Gamma(z)=\int_{-\infty}^{\infty}\frac{\rho(\varepsilon)d\varepsilon}{z+\varepsilon}\,, \tag{3·16}$$

and we use the semi-elliptical density of states Eq. (2·49) to model the valence band.

In order to reduce the number of free parameters we have assumed in Eq. (3·15) that the covalent contributions to the crystal field splitting are not affected in going from O_h to D_{4h} so that the $e_g(O_h)$ derived states (b_1, a_1) mix with an e_g transfer integral (V_e) and the other states with a $t_{2g}(O_h)$ transfer integral. We account for the additional splittings in D_{4h} by the electrostatic parameters Ds and Dt.[43] The hybridization energy δ and the d-hole count $\langle n_d\rangle$ of the $^2B_1$ ground state are found from

$$\begin{aligned}
&\delta=V_e^{\,2}\int\frac{\rho(\varepsilon)}{\delta-\Delta-\varepsilon}d\varepsilon\,,\\
&\langle n_d\rangle=\left(1+V_e^{\,2}\frac{\rho(\varepsilon)}{(\delta-\Delta-\varepsilon)^2}d\varepsilon\right)^{-1}
\end{aligned} \tag{3·17}$$

In Fig. 5 we show results for the (inverse) photoemission spectra of one-hole compounds obtained in this way. We used for the single particle parameters $\Delta=4$ eV, $W=4$ eV, $V_e=2$ eV, $V_t=1$ eV, $Dq=0.1$ eV, $Ds=0.1$ eV and $Dt=0.05$ eV. This

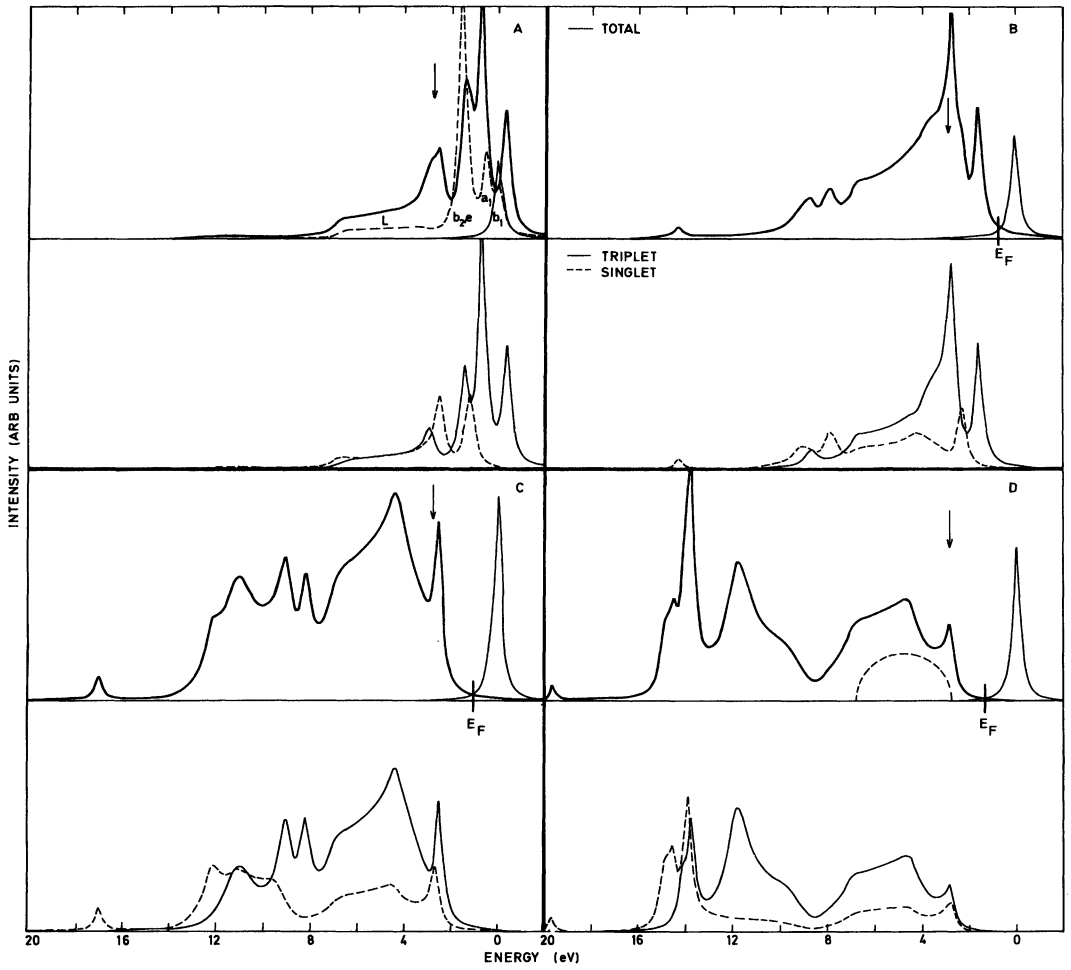

Fig. 5. Results for the photoemission (heavy line) and inverse photoemission (solid line) spectra for $\Delta = 4$ and $A = 0$(A), 3(B), 6(C) and 9(D) eV. The arrows indicate the onset of the ligand band. Also indicated are the triplet and singlet components of the photoemission spectrum (lower figures). In (A) we show the independent particle spectrum and in (D) the model DOS used for the ligand band (dashed lines).

results in an independent particle spectrum as indicated in Fig. 5(A) with the dashed line ('lifetime' broadening 0.4 eV FWHM). We obtained theoretical spectra including the d-d correlation effects by using for the Racah parameters $B = 0.15$ eV and $C = 0.75$ eV and we varied A ($A = 0, 3, 5, 9$ eV in Figs. 5(A)~(D)) which is equivalent to varying F_0 (B and C are expected to be insensitive to screening effects[13]). In the lower part of the figures we also indicate the contributions to the photoemission spectra from the singlet and triplet I.R.'s separately which are obtained by summing either the triplet- or the singlet I.R.'s in Eq. (3·12).

Focussing on the low energy end of the spectrum, the trend we discussed in § 2 is recognized. For large $A(=9\,\text{eV})$ it is seen that the low energy cutoff of the photoemission spectrum coincides with the threshold of the host valence band and in this case we have a charge transfer material (the C.T. gap magnitude $\Delta - (1/2)W + |\delta|$

is indicated by the arrow). If we lower A bound states are formed below the valence band threshold. In contrast to the results of § 2 more bound states can be found in the gap region due to the multiplet splittings. The distribution of these gap states resembles the distribution of the bare ionic d^8 multiplet. Considering for instance Fig. 5(C) it is seen that the triplet bound state is rather well bond while the singlet bound state is barely bound. On the other hand, the energy spread of the gap states is much smaller than the spread of the bare ionic multiplets. These are the essential characteristics of the multiple charge gap states as observed in semiconductor $3d$ impurity systems.[44] If A is further lowered (Fig. 5(A)) most of the d^8-terms can be distinguished above the valence band maximum although still their energy spread is sowewhat reduced compared to the bare ion by covalency effects. Note that we find for $A=0$ eV a negative $U_{\text{eff.}}$[44]

It is interesting to compare this to the high T_c's and recent calculations for CuO. The strong square planar like structure in these materials causes the transfer integral V_e to be a factor of $\sqrt{3}$ larger for the b_1 than the a_1 orbital. This is sufficient to cause the singlet state $^1A_1$ to be lower in energy than the triplet.[45] In this case the gap states are inverted in energy as compared to the d^8 states. This has important consequences for describing the high T_c's.[46]

Considering the overall aspects of the spectra it is seen that for increasing A the intensity is gradually moved to the high energy side of the spectrum which is a well-established trend.[16] For relatively small A (Fig. 5(B)) it is primarily the intensity in the ligand band region which is enhanced and for larger values of A ($A \geq \Delta$) a two-hole satellite starts to develop. Naively one would expect that the shape of this satellite would resemble the d^8 multiplet with a weight distribution given by the fractional parentage coefficients. The figure shows that this relationship is rather obscured in the parameter range investigated in the figure (compare Fig. 5(A) with Fig. 5(D)). The reason is that even for $A=9$ eV the real part of g_{dd}^{dd} is strongly varying in the energy region of the d^8 multiplet due to the presence of the $S(z)$ band (Eq. 2·41). The indirect mixing between the d^8 and the '$d^{10}\underline{L}^2$' states turns out to be sufficiently strong to obscure the ionic multiplet structure.

In order to apply this formalism to the (inverse) photoemission of Cu compounds we have to incorporate the emission of ligand p-electrons, which is quite important in

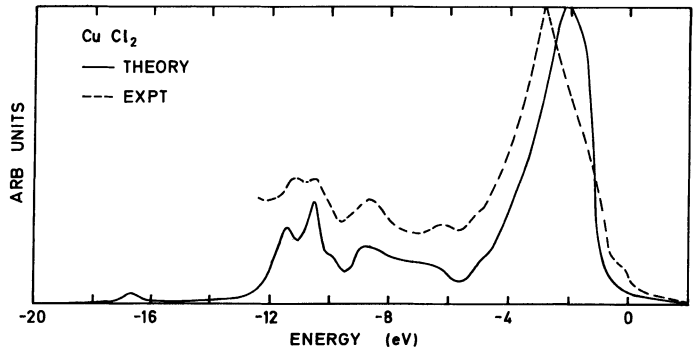

Fig. 6. Comparison of the experimental (HeII) photoemission spectrum of $CuCl_2$ (Ref. 25)) with a theoretical fit.

for instance the photoemission of Cu dihalides.[25] In Appendix B we show that this additional channel is easily incorporated using the two-hole Green's function technique. In Fig. 6 we compare the experimental spectrum of $CuCl_2$ ($h\omega=42$ eV) as obtained by van de Laan[25] with a theoretical result derived from Eqs. (B·5)~(B·7) where we used Eqs. (3·15)~(3·17) to model the one-hole Green's functions and a semi-elliptical band ($\rho(\varepsilon)$) with width $W=3$ eV to model the valence band.

In the experimental result we see a structured two-hole satellite centered at ≈ -11 eV and a broad, band-like feature at low energy. In order to reproduce this theoretically we used $A=6.5$ eV and $\Delta=2$ eV, together with $V_e=1.7$ eV. The absolute magnitudes of A and Δ are uncertain because the line shape is primarily sensitive to the difference between these parameters. In order to determine these parameters we need also the band gap magnitude which is unknown (with this choice $E_{\text{gap}}\approx 1$ eV, $\langle n_d\rangle\approx 0.7$). Also with respect to the crystal field parameters additional (band-structure, optical) data would be quite helpful. The values we used for these ($V_e/V_t=1.9$, $Dq=0.05$ eV, $Ds=0.1$ eV, $Dt=0.05$ eV) should be regarded as rough estimates because these only affect the detail of the (satellite) line shape.

The low energy region corresponds with the charge-transfer band according to the calculation. We used for the Cl $3p$ and Cu $3d$ photoemission amplitudes the ionic ratio $A_L/A_d=-0.45$[25] and we assumed these channels to be coherent (see Appendix B). We note that this assumption together with the sign of this ratio mainly affects the detail valence band shape for this choice of the parameters. The most significant aspect of the Cl $3p$-emission is that it changes the satellite main band intensity ratio drastically, compared to the $3d$ only spectra (see Fig. 11). The reason for this is that the $3d$ weight is spread over the full energy range while the $3p$ weight is limited to the valence band region and a relatively small increase of the $3p$ cross section gives then rise to a large increase of the satellite main line ratio.

In conclusion, we have shown that the photoemission spectrum of $CuCl_2$ gives strong evidence in favour of the charge transfer nature of this compound.

§ 4. Approximate method for many-hole problems

For most of the compounds we have to handle a large number of holes in order to calculate the ground state and the spectral functions. As we argued, the two-hole Green's function method is not useful in these cases and an alternative is the brute force expansion of § 2.b. In principle this expansion could be used to obtain exact results, also if multiplet effects are included. Such a calculation is however very tedious and, considering the inaccuracies introduced by the use of model-Hamiltonians, we can live with some loss of accuracy. Making use of the large numbers in the problem (U, and to some extent Δ) reasonably accurate results can be obtained by introducing some approximations which simplify the calculations greatly.

The first approximation is the neglect of d^{n+2} (and higher lying) states in the ground state calculation. These are at least at an energy $2\Delta+U$ compared to the d^n state and for the usual values of U and Δ found in TM compounds these can be safely neglected. The ground state is then calculated using the $|d^n\rangle$ and $|d^{n+1}\varepsilon\rangle$ states as a basis. In some occasions more than one $|d^n\rangle$ multiplet has to be considered as for

instance in Co^{2+} in O_h (I.R. $^4T_1$). Because the d^{n+1} configuration is also subjected to termsplitting, the d^n states hybridize with a set of $|d^{n+1}\varepsilon\rangle$ continua. If Γ_0^0 is the ground state I.R. we can label these states and continua as

$$|i_0\rangle=|d^n\alpha;\,\Gamma_0^0\rangle\,,$$
$$|j_0\varepsilon\rangle=|d^{n+1}(\Gamma_{A\beta})\varepsilon_1;\,\Gamma_0^0\rangle\,, \tag{4·1}$$

where α labels the components of $d^n(\Gamma_0^0)$, $\Gamma_{A\beta}$ the components (β) of the d^{n+1} I.R.'s (Γ_A) and 1 refers to a single-hole representation. We will have non-zero electrostatic matrix elements involving the d^n states ($h_{i_0}^{i'_0}$)- as well as $|j_0\varepsilon\rangle$ states ($h_{j_0}^{j'_0}$, $\delta(\varepsilon-\varepsilon')$) and also transfer matrix elements between the states and continua

$$h_{i_0}^{j'_0}(\varepsilon)=\langle i_0|H|j_0\varepsilon\rangle=\sqrt{N_h}\,\langle d^n\alpha;\,\Gamma_0^0|\}d^{N+1}(\Gamma_{A\beta})\underline{k}_1;\,\Gamma_0^0\rangle\,V_1(\varepsilon)\,, \tag{4·2}$$

where N_h is the number of holes in the ground state and $\langle|\}\rangle$ is a (subshell) fractional parentage coefficient ($\underline{k}_i$ denotes a i-hole at infinity).

A problem consisting of a number of bound states coupling to a number of continua is easy to solve. Using the Dyson equation it can be shown[47),16)]

$$\langle i_0|G|i'_0\rangle=\hat{G}_{i_0}^{i'_0}(\Gamma_0^0)=g_{i_0}^{i_0}\delta_{i_0i'_0}+g_{i_0}^{i_0}\sum_{i''_0}\Big[h_{i_0}^{i''_0}+\sum_{j_0j'_0}\int d\varepsilon h_{i_0}^{j_0}(\varepsilon)g_{j_0}^{j'_0}(\varepsilon)h_{j_0}^{i''_0}(\varepsilon)\Big]G_{i''_0}^{i'_0}(\Gamma_0^0)\,, \tag{4·3}$$

where $G=(z-H)^{-1}$ and $g_k{}^k=\langle k|(z-H_0)^{-1}|k\rangle$ (H_0 is diagonal). We could repeat this procedure for all I.R.'s of the neutral state (Γ_0) and we showed before that the imaginary parts of these Green's functions ($G_{i_0}^{i_0}(\Gamma)$) directly relate to the d-d optical spectra.[30)] The ground state wave function of the system can be written as

$$|\Phi_0;\,\Gamma_0^0\rangle=\sum_{i_0}a_0(i_0)|i_0\rangle+\sum_{j_0}\int d\varepsilon b_0(j_0,\,\varepsilon)|j_0\varepsilon\rangle\,, \tag{4·4}$$

and the coefficients $a_0(i_0)$ and $b_0(j_0,\,\varepsilon)$ as well as the ground state energy (δ) can be determined using straightforward variational theory.[16)]

The calculation of the BIS spectrum can be simplified in a similar way by the neglect of $|d^{n+3}\varepsilon\varepsilon'\rangle$ states which is even a better approximation than the neglect of $|d^{n+2}\varepsilon\varepsilon'\rangle$ states in the ground state calculation. The photoemission problem is however less straightforward and we have to introduce a second approximation. Considering only d-emission we write

$$\begin{aligned}G_{dd}^{<}(\Gamma_0^0mm',\,z)&=\langle\Phi_0;\,\Gamma_0^0|d_m{}^+\bar{G}d_{m'}|\Phi_0;\,\Gamma_0^0\rangle\\&=\sum_{\Gamma_I}\langle\Phi_m(t=0);\,\Gamma_I|\hat{G}|\Phi_{m'}(t=0);\,\Gamma_I\rangle\,,\end{aligned} \tag{4·5}$$

where we projected the prepared state on the $N-1$ electron I.R.'s (Γ_I). These states can be written in a compact form as

$$|\Phi_m(t=0);\,\Gamma_I\rangle=\sum_{i_0,i}a(i_0,\,i)|i\rangle+\sum_{j_0,j}\int d\varepsilon b(j_0,\,j,\,\varepsilon)|j\varepsilon\rangle\,, \tag{4·6}$$

where (γ labels the components of $|d^{n-1};\,\Gamma_I\rangle$)

$$|i\rangle=|d^{n-1}\gamma;\Gamma_I\rangle\,,$$
$$|j\varepsilon\rangle=|d^n(\Gamma_{0\alpha})\varepsilon_1\Gamma_I\rangle\,, \tag{4·7}$$

and the coefficients in Eq. (4·6) are given by

$$a(i_0,i)=a_0(\alpha)\langle[d^n\alpha;\Gamma_0^0]\underline{k}_m;\Gamma_I|\}d^{n-1}\gamma;\Gamma_I\rangle\,,$$
$$b(j_0,j,\varepsilon)=b_0(j_0,\varepsilon)\langle[d^{n+1}(\Gamma_{A\beta})\underline{k}_1;\Gamma_0^0]\underline{k}_m;\Gamma_I|\}d^n(\Gamma_{0\alpha})\underline{k}_1;\Gamma_I\rangle\,. \tag{4·8}$$

In the ionized state we have non-diagonal matrix elements between the states in Eq. (4·7)

$$h_i^{\,i'}=\langle i|H|i'\rangle\,,$$
$$h_i^{\,j}(\varepsilon)=\langle i|H|j\varepsilon\rangle=\sqrt{N}_h+\langle d^{n-1}\gamma;\Gamma_I|\}d^n(\Gamma_{0\alpha})\underline{k}_1;\Gamma_I\rangle\,V_1(\varepsilon)\,, \tag{4·9}$$

and matrix elements between the $|j\varepsilon\rangle$ states, which are further coupled to $|d^{n+1}\varepsilon\varepsilon'\rangle$ states (see for instance Appendix A). In order to evaluate Eqs. (4·5) and (4·6) we use the folding-back procedure as introduced by Gunnarsson and Schönhammer.[16] We write the Hamiltonian in the 'ionic' basis as

$$H=H_0+H_1+H_2\,, \tag{4·10}$$

where H_0 contains the diagonal part of H, H_1 the matrix elements in Eq. (4·9) and H_2 the non-diagonal matrix elements between the $|j\varepsilon\rangle$ states and all the other states we did not consider explicitly. We have

$$G=(z-\delta+H)^{-1}=\tilde{G}+\tilde{G}H_1G\,,$$
$$\tilde{G}=(z-\delta+H_0+H_2)^{-1}=G_0+G_0H_2\tilde{G}\,,$$
$$G_0=(z-\delta+H_0)^{-1}\,. \tag{4·11}$$

Using Eq. (4·11) we find after some algebra[48] the compact expression for Eq. (4·5)

$$G_{dd}^{\zeta}(\Gamma_0^0mm',z)=\sum_{\Gamma_I}[\sum_{i,i'}(A_i+F_i)(A_{i'}+F_{i'})G_i^{\,i'}+B]\,, \tag{4·12}$$

where

$$A_i=\sum_{i_0}a(i_0,i)\,,$$
$$F_i=\sum_{j_0,j,j'}\iint d\varepsilon d\varepsilon'\,b(j_0,j,\varepsilon)\,\tilde{g}_{j\varepsilon}^{\,j\varepsilon'}h_{j'}^{\,1}(\varepsilon')\,,$$
$$B=\sum_{j_0,j_0',j,j'}\iint d\varepsilon d\varepsilon'\,b(j_0,j,\varepsilon)\,\tilde{g}_{j\varepsilon}^{\,j'\varepsilon'}b(j_0',j',\varepsilon')\,, \tag{4·13}$$

and the Green's functions $G_i^{\,i'}$ can be derived from

$$G_i^{\,i'}=\langle i|G|i'\rangle=g_i^{\,i}\delta_{ii'}+g_i^{\,i}\sum_{i''}\Big[h_i^{\,i''}+\sum_{jj'}\iint d\varepsilon d\varepsilon'\,h_i^{\,j}(\varepsilon)\,\tilde{g}_{j\varepsilon}^{\,j'\varepsilon'}h_{j'}^{\,i''}(\varepsilon')\Big]G_{i''}^{\,i'}\,, \tag{4·14}$$

where we defined

$$\tilde{g}_{j\varepsilon}^{\,j'\varepsilon'}=\langle j\varepsilon|\tilde{G}|j'\varepsilon'\rangle\,. \tag{4·15}$$

The problems are in the evaluation of Eq. (4·15). Due to the hybridization between the $|d^n\varepsilon\rangle$ and $|d^n\varepsilon\varepsilon'\rangle$ states these are non-diagonal in ε as may be inferred from the example in Appendix A. The rigorous (numerical) evaluation of Eq. (4·15) is tedious[16] and instead we aprroximate Eq. (4·15) as follows:

$$\tilde{g}_{j\varepsilon}^{j'\varepsilon'}=\langle d^n(\Gamma_0\alpha)\varepsilon_1;\,\Gamma_I|\tilde{G}|d^n(\Gamma_0'\alpha')\varepsilon_1';\,\Gamma_I\rangle$$
$$\approx G_\alpha^{\alpha'}(\Gamma_0\alpha;\,z-\delta+\varepsilon_L+\varepsilon)\delta(\varepsilon-\varepsilon')\,, \tag{4·16}$$

where

$$G_\alpha^{\alpha'}(\Gamma_0\alpha)\equiv\langle d^n\alpha;\,\Gamma_0|G|d^n\alpha';\,\Gamma_0\rangle,$$

which can be determined from Eq. (4·3) and these relate directly to the d-d optical spectra as we argued before. Using Eq. (4·16) it is straightforward to evaluate Eqs. (4·12)~(4·14).

In Eq. (4·16) we have assumed that the extra valence band hole in the ionized state can be viewed as a spectator with respect to the mixing of the $|d^n\rangle$ and $|d^{n+1}\varepsilon\rangle$ states. This automatically yields the exact result that the charge transfer gap magnitude equals $\Delta-(1/2)W+|\delta|$. In order to see how well it works in other respects we compare results obtained with this scheme for Cu(II) impurities with the exact results of § 2.b. In order to avoid irrelevant complication we have assumed octahedral (O_h) symmetry. The Green's functions in Eq. (4·3) are simply the one-hole Green's functions from Eq. (3·11) which we model as

$$G_e^e(z)=(z-V_e^2\Gamma(z+\Delta))^{-1}\,,$$
$$G_t^t(z)=(z+10Dq-V_t^2\Gamma(z+\Delta))^{-1}\,, \tag{4·17}$$

and the (^2E) ground state is found according to Eq. (3·17). The fractional parentage coefficients are easily determined and the g_i''s and $h_{ii'}$ can be determined from the electrostatic matrices as tabulated by Griffith.[42] We end up with

$$G_{dd}^<(^2E,\,z)=\sum_{mm'}G_{dd}^<(emm',\,z)\approx\sum_m G_{dd}^<(emm,\,z)$$
$$=\frac{9}{4}G_{et}^{et<}(^3T_1)+\frac{9}{4}G_{et}^{et<}(^3T_2)+\frac{3}{2}G_{e^2}^{e^2<}(^3A_2)$$
$$+\frac{3}{4}G_{et}^{et<}(^1T_1)+\frac{3}{4}G_{et}^{et<}(^1T_2)+G_{e^2}^{e^2<}(^1E)+\frac{1}{2}G_{e^2}^{e^2<}(^1A_1)\,, \tag{4·18}$$

where

$$G_{em}^{em<}(\Gamma_I)=\langle n_d\rangle[(1+A_m(z))^2G_{em}^{em}(\Gamma_I)+B_m(z)]\,,$$
$$A_m(z)=V_e^2\int\frac{d\varepsilon\rho(\varepsilon)}{\delta-\Delta-\varepsilon}G_m{}^m(z-\delta+\varepsilon_L+\varepsilon)\,,$$
$$B_m(z)=V_e^2\int\frac{d\varepsilon\rho(\varepsilon)}{(\delta-\Delta-\varepsilon)^2}G_m{}^m(z-\delta+\varepsilon_L+\varepsilon)\,, \tag{4·19}$$

and $G_{em}^{em}(\Gamma_I)$ can be derived from Eq. (4·14). We note that we omitted terms $G_{dd}^<(emm',\,z)$ with $m\neq m'$ in Eq. (4·18) to simplify matters further. Using the formal-

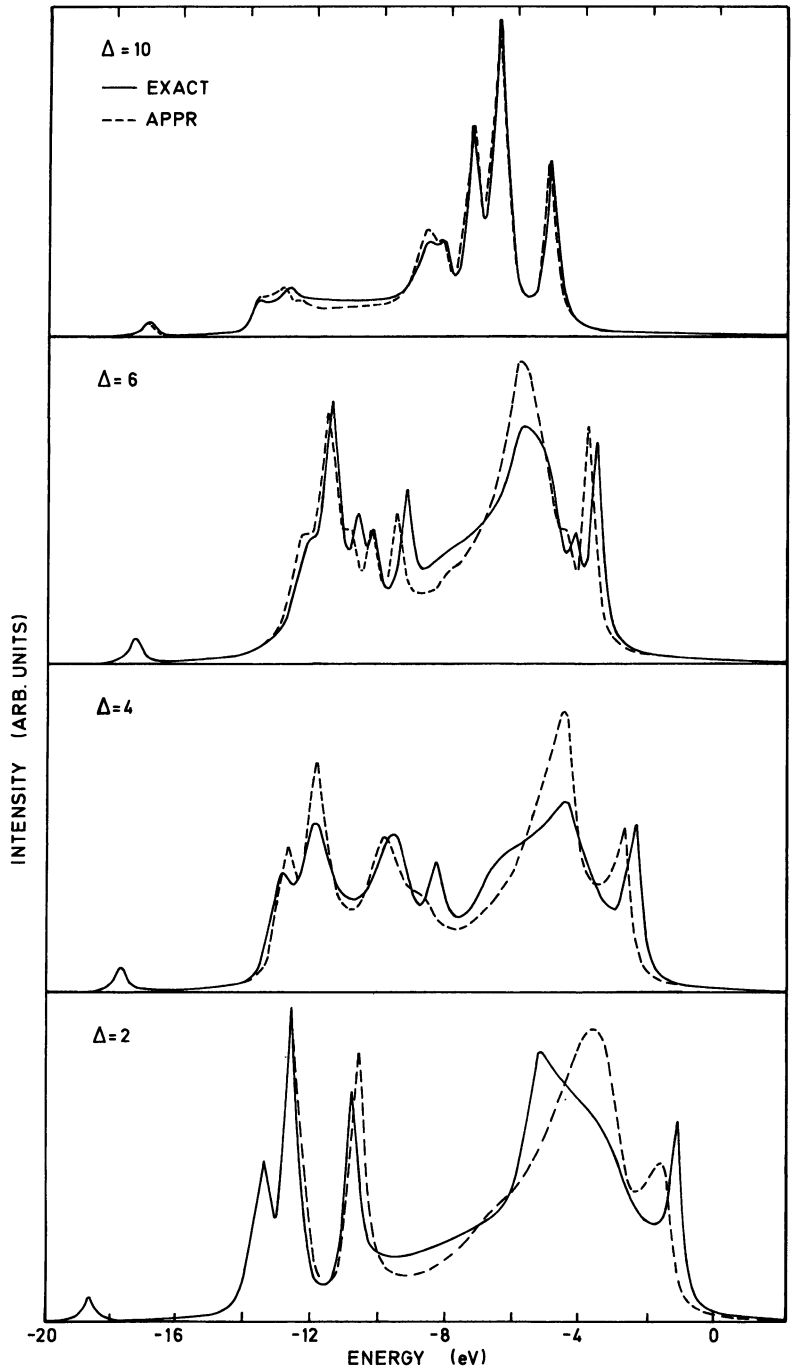

Fig. 7. Comparison of 'exact' photoemission line shapes (solid lines) with approximate results (dashed lines) for the one-hole impurities. Parameters are as in Fig. 5 except $A=7$ eV and Δ as indicated.

ism of § 2.b we also derived the 'exact' photoemission spectra and in Fig. 7 we compare these with the approximate results derived from Eqs. (4·18) and (4·19). We used the same parameters as in Fig. 5 except that $A=7$ eV and values for Δ as

indicated in the figure.

It can be seen from the figure that the approximated results mimic quite well the exact results. The major deviations are in the host valence band region and the results in Appendix B indicate that it is anyhow unrealistic to expect that the line shape in this region can be understood in full detail using model Hamiltonians. It is also seen that the binding energy of the bound gap states is sowewhat underestimated in the approximate results. In the approximation we used it is literally the case that for large U in the valence band region one hole is bound to the impurity while the other hole moves independently in the host valence band. The failure of the approximation indicates that this conception, as put forward in § 2.a, is somewhat oversimplified. It indicates that for non-integral valence the valence band hole interacts with the spin of the localized hole, although this interaction is, in the charge transfer regime, to small to bind the itinerant hole to the impurity.

§ 5. Application to nickel compounds

Recently the divalent Ni-compounds have been subject to several spectroscopic investigations. The $2p$-XPS,[12] XAS[13] and d-d optical spectra[30] of several of these compounds have been analyzed by us in the impurity model framework, from which we obtained already some insight in the electronic structure of these materials. Also the valence photoemission spectra of these are well documented,[49] especially the spectra of NiO[50),6),7] which will be analyzed in detail in this section.

The insulating Ni compounds are characterized by two-hole ground states. The ground state symmetry is usually ${}^3A_2$ (O_h) and the ground state wave function has the simple form under the neglect of $|d^{10}\varepsilon\varepsilon'\rangle$ states (see also Ref. 12))

$$|\Phi_0; {}^3A_2\rangle = a_0\left(|d^8; {}^3A_2\rangle + \int d\varepsilon b_0(\varepsilon)|d^9\varepsilon_e; {}^3A_2\rangle\right), \tag{5·1}$$

because no term splittings enter. We find for the ground state hybridization energy and coefficients

$$\delta = 2V_e^2 \int \frac{\rho(\varepsilon)d\varepsilon}{\delta - \Delta - \varepsilon},$$

$$|a_0|^2 = \left(1 + 2V_e^2 \int d\varepsilon \rho(\varepsilon)(\delta - \Delta - \varepsilon)^{-2}\right)^{-1},$$

$$b_0(\varepsilon) = \sqrt{2}\, V_e a_0 \rho^{1/2}(\varepsilon)(\delta - \Delta - \varepsilon)^{-1}. \tag{5·2}$$

The inverse photoemission spectrum is a simple one-hole problem which can be calculated in the space spanned by the $|d^9\rangle$ and $|d^{10}\varepsilon_e\rangle$ states. The latter states are at high energy ($\Delta + U$) and to be consistent with the approximation for the ground state it is better to neglect these. The inverse photoemission spectrum consists then of a single line at $\varepsilon_d + J({}^3A_2) + |\delta|$ ($J({}^3A_2)$ is the exchange stabilization of the $|d^8; {}^3A_2\rangle$ state) and weight $|a_0|^2$ if only the filling of d states is considered.

The calculation of the photoemission spectra is a three-hole problem and is therefore less trivial. We calculate these using the method of the previous section.

Table II. States and matrix elements used in the calculation of the photoemission spectrum of NiO.

$^2T_1$

$|1\rangle=|t_2^3\rangle$, $|2\rangle=|t_2^2(^3T_1)e\rangle$, $|3\rangle=|t_2^2(^1T_2)e\rangle$, $|4\rangle=|t_2e^2(^3A_2)\rangle$, $|5\rangle=|t_2e^2(^1E)\rangle$,
$|6\rangle=|t_2^2(^1E)k_t\rangle$, $|7\rangle=|e^2(^1E)k_t\rangle$, $|8\rangle=|e^2(^3A_2)k_t\rangle$, $|9\rangle=|t_2^2(^3T_1)k_e\rangle$,
$|10\rangle=|et_2(^3T_1)k_e\rangle$, $|11\rangle=|t_2^2(^3T_1)k_t\rangle$, $|12\rangle=|et_2(^3T_1)k_t\rangle$, $|13\rangle=|et_2(^3T_2)k_e\rangle$,
$|14\rangle=|et_2(^3T_2)k_t\rangle$, $|15\rangle=|et_2(^1T_1)k_e\rangle$, $|16\rangle=|et_2(^1T_1)k_t\rangle$, $|17\rangle=|t_2^2(^1T_2)k_e\rangle$,
$|18\rangle=|et_2(^1T_2)k_e\rangle$, $|19\rangle=|t_2^2(^1T_2)k_t\rangle$, $|20\rangle=|et_2(^1T_2)k_t\rangle$, $|a\rangle=|e^2(^3A_2)\rangle$,
$|b\rangle=|ek_e(^3A_2)\rangle$

$\langle 1\|6\rangle=-V_t$, $\langle 1\|11\rangle=V_t\sqrt{3/2}$, $\langle 1\|19\rangle=V_t/\sqrt{2}$, $\langle 2\|9\rangle=V_e$, $\langle 2\|12\rangle=-\sqrt{3/8}$,
$\langle 2\|14\rangle=V_t/\sqrt{8}$, $\langle 2\|16\rangle=3V_t/\sqrt{8}$, $\langle 2\|20\rangle=-V_t\sqrt{3/8}$, $\langle 3\|12\rangle=-V_t\sqrt{3/8}$,
$\langle 3\|14\rangle=-3V_t/\sqrt{8}$, $\langle 3\|16\rangle=-V_t/\sqrt{8}$, $\langle 3\|17\rangle=V_e$, $\langle 3\|20\rangle=-V_t\sqrt{3/8}$,
$\langle 4\|8\rangle=V_t$, $\langle 4\|10\rangle=-V_e/2$, $\langle 4\|13\rangle=V_e/2$, $\langle 4\|15\rangle=-V_e\sqrt{3/4}$, $\langle 4\|18\rangle=V_e\sqrt{3/4}$,
$\langle 5\|7\rangle=V_t$, $\langle 5\|10\rangle=V_e\sqrt{3/4}$, $\langle 5\|13\rangle=V_e\sqrt{3/4}$, $\langle 5\|15\rangle=-V_e/2$, $\langle 5\|18\rangle=-V_e/2$.

$\langle a\|t_\downarrow\|4\rangle=-\sqrt{2/3}$, $\langle b\|t_\downarrow\|10\rangle=1/\sqrt{12}$, $\langle b\|t_\downarrow\|13\rangle=-1/\sqrt{12}$,
$\langle b\|t_\downarrow\|15\rangle=1/2$, $\langle b\|t_\downarrow\|18\rangle=-1/2$

$^4T_1$

$|1\rangle=|t_2^2(^3T_1)e\rangle$, $|2\rangle=|t_2e^2(^3A_2)\rangle$, $|3\rangle=|t_2^2(^3T_1)k_t\rangle$, $|4\rangle=|et(^3T_1)k_t\rangle$,
$|5\rangle=|t_2^2(^3T_1)k_t\rangle$, $|6\rangle=|et_2(^3T_2)k_t\rangle$, $|7\rangle=|e_2^2(^3A_2)k_t\rangle$, $|8\rangle=|et_2(^3T_1)k_e\rangle$,
$|9\rangle=|et_2(^3T_2)k_e\rangle$,

$\langle 1\|3\rangle=V_e$, $\langle 1\|4\rangle=V_t\sqrt{3/2}$, $\langle 1\|6\rangle=V_t/\sqrt{2}$, $\langle 2\|7\rangle=V_t$, $\langle 2\|8\rangle=V_e$,
$\langle 2\|9\rangle=-V_e$,

$\langle a\|t_\uparrow\|2\rangle=1$, $\langle b\|t_\uparrow\|8\rangle=1/\sqrt{2}$, $\langle b\|t_\uparrow\|9\rangle=-1/\sqrt{2}$, $\langle a\|t_\downarrow\|2\rangle=1/\sqrt{3}$,
$\langle b\|t_\downarrow\|8\rangle=1/\sqrt{6}$, $\langle b\|t_\downarrow\|9\rangle=-1/\sqrt{6}$

^2E

$|1\rangle=|e^3\rangle$, $|2\rangle=|t_2^2(^1E)e\rangle$, $|3\rangle=|t_2^2(^1A_1)e\rangle$, $|4\rangle=|t_2^3\rangle$, $|5\rangle=|e^2(^3A_2)k_e\rangle$,
$|6\rangle=|e^2(^1E)k_e\rangle$, $|7\rangle=|t_2^2(^1E)k_e\rangle$, $|8\rangle=|e^2(^1A_1)k_e\rangle$, $|9\rangle=|t_2^2(^1A_1)k_e\rangle$,
$|10\rangle=|et_2(^3T_2)k_t\rangle$, $|11\rangle=|et_2(^1T_2)k_t\rangle$, $|12\rangle=|t_2^2(^1T_2)k_t\rangle$, $|13\rangle=|et_2(^3T_1)k_t\rangle$,
$|14\rangle=|t_2^2(^3T_1)k_t\rangle$, $|15\rangle=|et_2(^1T_1)k_t\rangle$, $|16\rangle=|e^3(^3A_2)k_e\rangle$,

$\langle 1\|5\rangle=V_e\sqrt{3/2}$, $\langle 1\|6\rangle=V_e$, $\langle 1\|8\rangle=V_e/\sqrt{2}$, $\langle 2\|7\rangle=-V_e$, $\langle 2\|10\rangle=V_t\sqrt{3/4}$,
$\langle 2\|11\rangle=V_t/2$, $\langle 2\|13\rangle=-V_t\sqrt{3/4}$, $\langle 2\|15\rangle=-V_t/2$, $\langle 3\|9\rangle=V_e$,
$\langle 3\|10\rangle=V_t\sqrt{3/4}$, $\langle 3\|11\rangle=V_t/2$, $\langle 3\|13\rangle=V_t\sqrt{3/4}$, $\langle 3\|15\rangle=V_t/2$,
$\langle 3\|12\rangle=V_t\sqrt{3/2}$, $\langle 3\|14\rangle=-V_t\sqrt{3/2}$,

$\langle a\|e_\downarrow\|1\rangle=1$, $\langle b\|e_\downarrow\|5\rangle=1/\sqrt{12}$, $\langle b\|e_\downarrow\|6\rangle=1/\sqrt{2}$, $\langle b\|e_\downarrow\|8\rangle=1/2$,
$\langle b\|e_\downarrow\|16\rangle=-1/\sqrt{6}$

A nice feature of this method is the direct use which can be made of the information obtained from the optical spectra. We presented a detailed analysis of the d-d excitons using the 'exact' two-hole Green's function formalism elsewhere.[30] As it turns out, essentially the same results are found if the d^{10} states are neglected and we used Eq. (4·3) to calculate the two-hole Green's functions needed as an input for the photoemission calculation. Finally we need the electrostatic matrices of d^7 ($h_t^{i'}$ in Eq. (4·14)) which can be found in Griffith's book[42] and the fractional parentage coefficients (Eqs. (4·8) and (4·9)) which are summarized in Table II. These are determined in the electron gauge according to the phase conventions of Griffith and

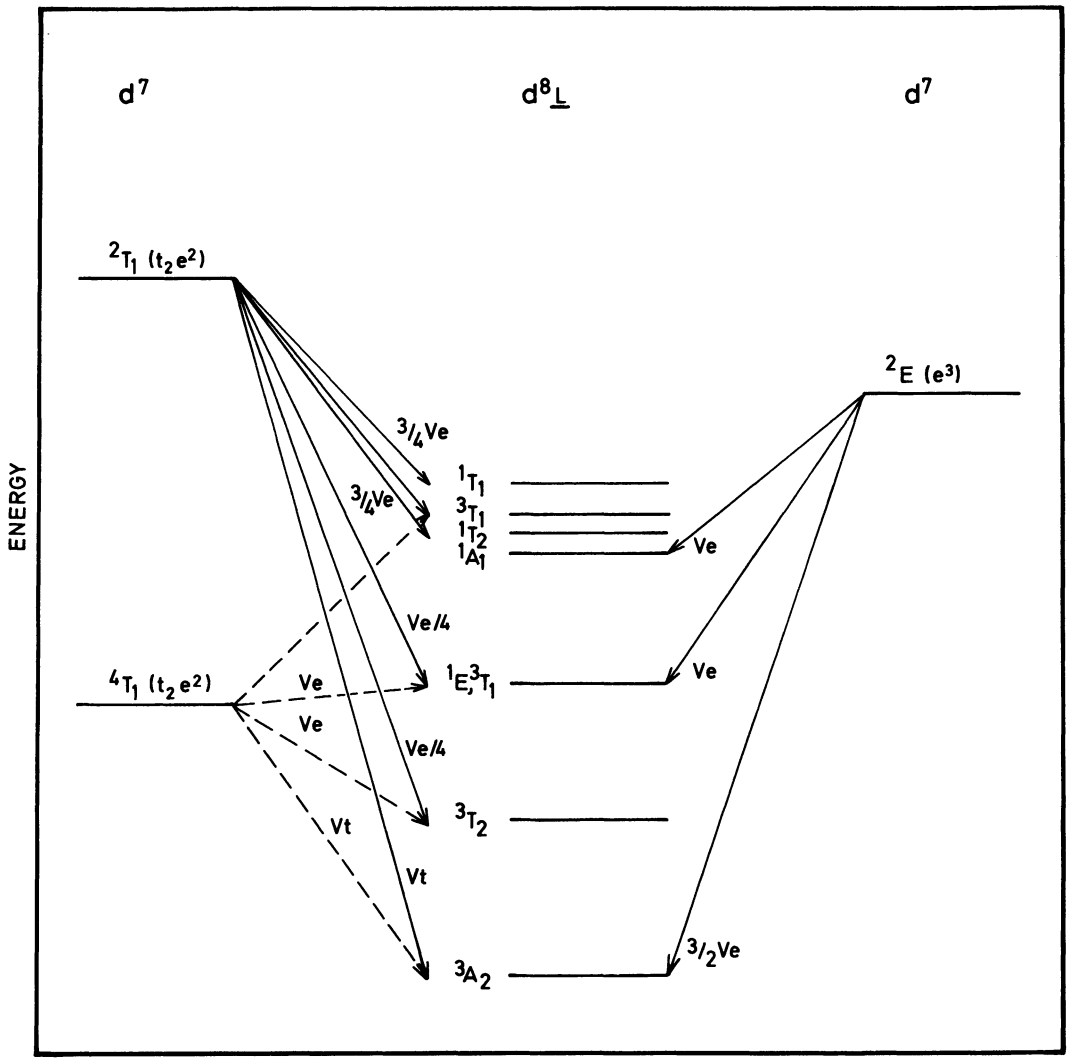

Fig. 8. Summary of the most important d^7 states and $d^8\underline{L}$ continua in the approximate calculation of the photoemission spectrum of divalent Ni-compounds.

therefore the electrostatic matrices for d^2 and d^3 have to be used.

In Fig. 8 we summarize the most important states and couplings as present in the calculation of the photoemission spectrum. Only the ${}^4T_1$, ${}^2T_1$ and ${}^2E$ three-hole I.R.'s are accessible by the removal of a d electron from the ${}^3A_2$ ground state. We have then to handle resp. 2-, 4- and 5- dimensional electrostatic matrices for d^7 and in the figure we only indicate the strong field components of d^7 which are directly populated in the photoemission process. We indicate also the thresholds of the $|d^8\varepsilon\rangle$ bands and the hybridization matrix elements between these and the d^7 terms. Already on this level the picture is complicated but using Eqs. (4·12)~(4·14) all these contributions are easily collected and the lengthy expression obtained in this way can be evaluated numerically.

Because the information in the optical spectra can be used we can get rid of all

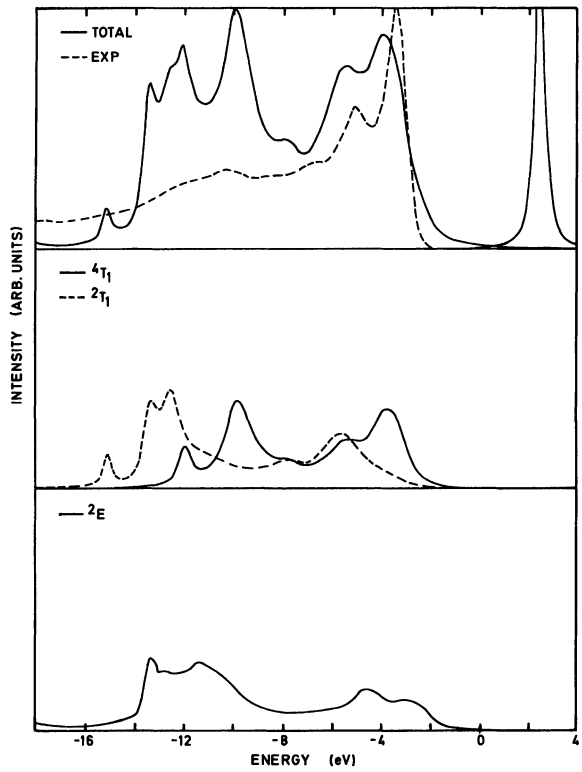

Fig. 9. Photoemission/inverse photoemission spectrum for 'optical' parameters and $A=8.5$ eV compared to the experimental spectrum of NiO (Ref. 48)). The contribution of different IR's to the photoemission spectrum are also indicated.

one-particle parameters. Using $B=0.13$ eV and $C=0.6$ eV for the Ni^{2+} (d^8) racah parameters a reasonable fit for the optical spectrum of NiO is found using $\Delta=5.5$ eV, $V_e=1.6$ eV, $V_t=0.6$ eV and $Dq=0.7$ eV. We modelled $\rho(\varepsilon)$ after the O2p DOS obtained from bandstructure calculation (see inset Fig. 9).[18] The only free parameters left are the d^7-Racah parameters. We can rely on free ion values for the B and C parameters ($B=0.14$ eV and $C=0.68$ eV[26]) and only A (d^7-d^9) has to be determined by comparison with experiment. The main line-satellite splitting is determined by $A-\Delta$ and in this way we find $A=8.5$ eV for NiO and the spectrum obtained is indicated in Fig. 9. This result is compared in the figure with the experimental spectrum obtained by Oh et al. ($\hbar\omega=120$ eV).[50] It is seen that the agreement between theory and experiment is poor. First we note that the satellite in the theoretical spectrum is much too large. One could argue that is due to the neglect of O2p-emission (see Appendix B), but this seems unlikely because it is known[26] that the O2p cross section is relatively low compared to the Ni3d cross section at high photon energy. A second major discrepancy is the band-like appearance of the main line in the theoretical spectrum which badly compares with the sharp peak seen in the experimental spectrum.

Apparently it is not possible to model the neutral and charged system with exactly the same effective Hamiltonian. This is not surprising because in the real system many more, relatively small, interactions are present which are neglected in our model Hamiltonian. In the analysis of the core spectra we faced a similar problem. We found there[12] that smaller transfer integrals had to be used in the $2p$-XAS final state compared to the transfer integrals in the (charged) final states of the $2p$-XPS process. We argued that in the Anderson model Coulomb interactions are neglected of the form

$$\Delta T=\langle \underline{c}d|\frac{1}{r_{12}}|\underline{c}L\rangle\,, \tag{5·3}$$

where $\underline{c}$ is a core-hole and L a ligand electron. These will cause an increase of the effective transfer integral. Assuming a screening length significantly larger than the interatomic separation, which is realistic for insulators, we estimated this interaction to be of the order of 0.5 eV. We showed in Ref. 12) that this modest transfer integral renormalization has a large impact on the spectral line shapes. We note that in more covalent materials ΔT has the opposite sign.[51]

The d-wave functions have a rather small radial extent and also in the photoemission final state such an effect is expected, affecting mainly the magnitude of the

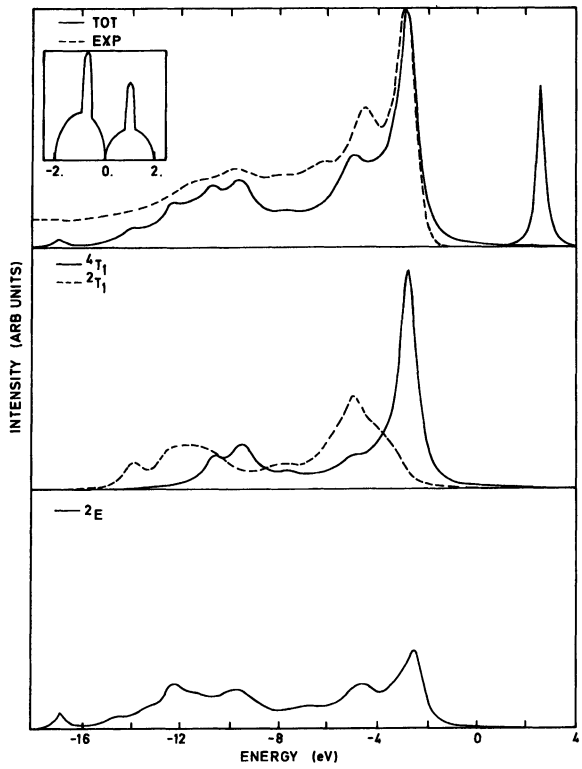

Fig. 10. As Fig. 9 but now with an enhanced d^7-$d^8\underline{L}$ hybridization and A=6.5 eV. In the inset we show the DOS used to model the ligand band.

$\langle d^7|H|d^8\varepsilon\rangle$ transfer integrals. In Fig. 10 we show the results obtained by increasing these transfer integrals by a factor of 1.4. In order to reproduce the main line satellite splitting we had to reduce A to a value of 6.5 eV and $10Dq$ by 0.3 eV. The other parameters were kept the same. The reduction of $10Dq$ seems to us barely significant because it is expected that in this region the O2p emission (which we neglected) is quite important. Again it is observed that a modest increase of some transfer integrals has a large effect on the line shape, which is mainly due to the large degeneracy factors N_h+1 which amplify the one-body transfer integrals in a many-body calculation. The satellite intensity has dropped down to an acceptable magnitude and it is even more significant that a (nearly) bound state is now found at threshold.

It is interesting that according to the calculation the relative orientations of the impurity spin and the spin of the hole is of great importance. We also noticed such an effect in § 3 and it is clear that this is due to the large termsplittings in the d^7 manifold. Because the d^7 $^4T_1$ states are at relatively low energy a bound state of $^4T_1$ symmetry is pushed out of the valence band while the low energy doublet states are still of charge-transfer nature because these d^7 states are at much higher energy. As a result, the main line is quartet d^7 like (NiO is well inside the intermediate regime) and the shoulder corresponds with charge tranfer ($\approx|d^8\varepsilon\rangle$) doublet states. Considering the resonant photoemission behaviour it is expected that the d^7-like state will show a much more pronounced anti-resonance behaviour than the charge-transfer like shoulder. This is actually seen in the EDC's obtained by Oh et al.[50] where the main line intensity becomes comparable in magnitude to the shoulder at resonance.

Because of the importance of the ligand p emission in the Ni-dihalides we have not attempted to produce quantitative fits for the photoemission of these materials. However, some observations can be made. If we compare the photoemission spectra of NiO and for instance $NiCl_2$[49] it is observed that the main line-satellite splitting is considerable smaller in the latter case, while the conductivity gaps are similar.[6),52] Hüfner suggested, based on this observation that the U in $NiCl_2$ would be considerably smaller compared to the finding for NiO.[53] However, it can also be observed that the appearance of the main line in $NiCl_2$ is much more band-like than in NiO which indicates that this material is well inside the charge-transfer regime. This is confirmed by the resonant photoemission measurements where no significant change in resonance behaviour is seen for different points in the main band. This together with the reduced mainline satellite splitting, indicates that the transfer integrals are smaller in $NiCl_2$ compared to NiO, which is not surprising. We found in fact that a reduction of the V's by 20% keeping the other parameters the same, can account for the differences between the photoemission spectra of $NiCl_2$ and NiO.

§ 6. Conclusion and final remarks

In this paper we have presented a new way of looking at the valence electronic structure of TMC's based on the neglect of the dispersional width of the d-bands. In this way we arrived at a classification scheme for the band gaps in these compounds (charge-transfer, intermediate and Mott-Hubbard gaps) and we presented direct

evidence for the validity of these ideas by a detailed analysis of the (inverse) photoemission spectra of $CuCl_2$ and NiO. This scheme gives us a basis to understand the systematics of the valence electronic structure of TMC's. As we show elsewhere[48),55)] it is indeed possible to account for all known band-gap trends of at least the divalent insulating compounds within this scheme.

The theory is also suggestive with respect to the nature of the carriers in these materials. Focussing on the late $3d$-compounds it is expected that in nearly all cases the electron move in the narrow 'd^{n+1}' like bands. On the other hand, the hole mass is expected to decrease for decreasing anion electronegatively. In the charge-transfer regime the holes are much lighter than the electrons and the conduction is expected to be exclusively p-type. This has been confirmed recently by photoconductivity measurements on the (charge-transfer) Ni-dihalides.[52)] Other examples are the semimagnetic semiconductors like $Cd_{1-x}Mn_xTe$ where the holes are known to be of Te $5p$ character,[55)] although in these cases the electrons are also light because of the small host bandgap.

Some points deserve further attention. Although the neglect of the dispersional width of the d-bands is certainly allowed if the high energy scale is considered it is necessary to include the translational symmetry of the TM-ions to get a more precise description of the low energy quasi-particles in this materials. This is not only of academic interest. In recent studies Sternberg et al.[28)] Shen et al., and Brooks et al.[29)] identified dispersion in the d like bands with angular resolved photoemission. A promising approach to study these questions seems to be the canonical perturbation expansion introduced by Chao et al. some time ago in the study of the Hubbard Hamiltonian.[39)]

As in the case of the core-spectra[12),13)] we found again that the parameters have to be altered as the system is perturbed by ionization, which points at the incompleteness of the effective Hamiltonian used by us. We find, as for the core-spectra, that the discrepancies are removed when we allow for a relatively modest renormalization of the effective hybridization. In order to investigate this problem better first principle calculation could be of great help. In any case, it is a quite significant development that both first principle quantum chemical cluster calculations[56)] and local density supercell calculations[57)] obtain parameters close to those in our semi-empirical picture.

Acknowledgements

We gratefully acknowledge helpful discussions with J. W. Allen, C. Haas, O. Gunnarsson, G. J. M. Janssen, W. C. Nieuwpoort, A. M. Oleś and H. Tjeng. This investigation was supported by the Netherlands Foundation for Chemical Research (SON) with financial aid from the Netherlands Organization for the Advancement of Pure Research (ZWO).

Appendix A

In this appendix we present a survey of the states and matrix elements used in the

gap calculation for large degeneracy of § 2.

We have for the N electon problem

$$|d^n\rangle = d_1 d_2 |d^{n+2}\rangle ,$$

$$|d^{n+1}\varepsilon\rangle = \frac{1}{\sqrt{2}}(d_1 c_{\varepsilon 2} + c_{\varepsilon 1} d_2)|d^{n+2}\rangle ,$$

$$|d^{n+2}\varepsilon\varepsilon\rangle = c_{\varepsilon 1} c_{\varepsilon 2} |d^{n+2}\rangle ,$$

$$|d^{n+2}\varepsilon\varepsilon'\rangle = \frac{1}{\sqrt{2}}(c_{\varepsilon 1} c_{\varepsilon' 2} + c_{\varepsilon' 1} c_{\varepsilon 2})|d^{n+2}\rangle , \quad (\varepsilon < \varepsilon') \tag{A·1}$$

with matrix elements

$$\langle d^n|H|d^n\rangle = 0 , \quad \langle d^{n+1}\varepsilon|H|d^{n+1}\varepsilon\rangle = \Delta + \varepsilon ,$$

$$\langle d^{n+2}\varepsilon\varepsilon'|H|d^{n+2}\varepsilon\varepsilon'\rangle = 2\Delta + U + \varepsilon + \varepsilon'$$

and

$$\langle d^n|H|d^{n+1}\varepsilon\rangle = \sqrt{2}\, V(\varepsilon) ,$$

$$\langle d^{n+1}\varepsilon|H|d^{n+2}\varepsilon\varepsilon\rangle = \sqrt{2}\, V(\varepsilon) ,$$

$$\langle d^{n+1}\varepsilon|H|d^{n+2}\varepsilon\varepsilon'\rangle = V(\varepsilon') , \quad \langle d^{n+1}\varepsilon'|H|d^{n+2}\varepsilon\varepsilon'\rangle = V(\varepsilon) . \tag{A·2}$$

We note that for $N_\varepsilon \to \infty$ states like $|d^n\varepsilon\varepsilon'\rangle$ $(\varepsilon = \varepsilon')$ have a vanishing contribution. For $N_\varepsilon = 30$ however they have still some (small) influence.

The $N+1$ electron problem is trivial

$$|d^{n+1}\rangle = d_1 |d^{n+2}\rangle ,$$

$$|d^{n+2}\varepsilon\rangle = c_{\varepsilon 1} |d^{n+2}\rangle \tag{A·3}$$

with matrix elements

$$\langle d^{n+1}|H|d^{n+1}\rangle = \varepsilon_{d'} \langle d^{n+2}\varepsilon|H|d^{n+2}\varepsilon\rangle = \varepsilon_d + \Delta + U + \varepsilon , \quad \langle d^{n+1}|H|d^{n+2}\varepsilon\rangle = V(\varepsilon) .$$

The $N-1$ electron problem is evaluated in the basis

$$|d^{n+1}\rangle = d_1 d_2 d_3 |d^{n+2}\rangle ,$$

$$|d^n\varepsilon\rangle = \frac{1}{\sqrt{3}}(d_1 d_2 c_{\varepsilon 3} + d_1 c_{\varepsilon 2} d_3 + c_{\varepsilon 1} d_2 d_3)|d^{n+2}\rangle ,$$

$$|d^{n+1}\varepsilon\varepsilon\rangle = \frac{1}{\sqrt{3}}(d_1 c_{\varepsilon 2} c_{\varepsilon 3} + c_{\varepsilon 1} d_2 c_{\varepsilon 3} + c_{\varepsilon 1} c_{\varepsilon 2} d_3)|d^{n+2}\rangle ,$$

$$|d^{n+1}\varepsilon\varepsilon'\rangle = \frac{1}{\sqrt{6}}(d_1 c_{\varepsilon 2} c_{\varepsilon' 3} + d_1 c_{\varepsilon' 2} c_{\varepsilon 3} + c_{\varepsilon 1} d_2 c_{\varepsilon' 3}$$

$$+ c_{\varepsilon' 1} d_2 c_{\varepsilon 3} + c_{\varepsilon 1} c_{\varepsilon' 2} d_3 + c_{\varepsilon' 1} c_{\varepsilon 2} d_3)|d^{n+2}\rangle ,$$

$$|d^{n+2}\varepsilon\varepsilon\varepsilon\rangle = c_{\varepsilon 1} c_{\varepsilon 2} c_{\varepsilon 3} |d^{n+2}\rangle ,$$

$$|d^{n+2}\varepsilon\varepsilon'\rangle=\frac{1}{\sqrt{3}}(c_{\varepsilon 1}c_{\varepsilon 2}c_{\varepsilon' 3}+c_{\varepsilon 1}c_{\varepsilon' 2}c_{\varepsilon 3}+c_{\varepsilon' 1}c_{\varepsilon 2}c_{\varepsilon 3})|d^{n+2}\rangle\,,\quad(\varepsilon<\varepsilon')$$

$$|d^{n+2}\varepsilon\varepsilon'\varepsilon''\rangle=\frac{1}{\sqrt{6}}(c_{\varepsilon 1}c_{\varepsilon' 2}c_{\varepsilon'' 3}+c_{\varepsilon 1}c_{\varepsilon'' 2}c_{\varepsilon' 3}+c_{\varepsilon' 1}c_{\varepsilon 2}c_{\varepsilon'' 3}$$
$$+c_{\varepsilon'' 1}c_{\varepsilon 2}c_{\varepsilon' 3}+c_{\varepsilon' 1}c_{\varepsilon'' 2}c_{\varepsilon 3}+c_{\varepsilon'' 2}c_{\varepsilon' 1}c_{\varepsilon 3})|d^{n+2}\rangle\,,\quad(\varepsilon<\varepsilon'<\varepsilon'')\,.\qquad(\text{A}\cdot 4)$$

We have for the diagonal matrix elements $\langle d^{n-1}|H|d^{n-1}\rangle=U-\Delta+\varepsilon_L$, $\langle d^n\varepsilon|H|d^n\varepsilon\rangle=\varepsilon_L+\varepsilon$, $\langle d^{n+1}\varepsilon\varepsilon'|H|d^{n+1}\varepsilon\varepsilon'\rangle=\varepsilon_L+\Delta+\varepsilon+\varepsilon'$, $\langle d^{n+2}\varepsilon\varepsilon'\varepsilon''|H|d^{n+2}\varepsilon\varepsilon'\varepsilon''\rangle=\varepsilon_L+2\Delta+U+\varepsilon+\varepsilon'+\varepsilon''$ and for the non-diagonal matrix elements

$$\langle d^{n-1}|H|d^n\varepsilon\rangle=\sqrt{3}\,V(\varepsilon)\,,$$
$$\langle d^n\varepsilon|H|d^{n+1}\varepsilon\varepsilon\rangle=2\,V(\varepsilon)\,,$$
$$\langle d^n\varepsilon|H|d^{n+1}\varepsilon\varepsilon'\rangle=\sqrt{2}\,V(\varepsilon')\,,\quad\langle d^n\varepsilon'|H|d^{n+1}\varepsilon\varepsilon'\rangle=\sqrt{2}\,V(\varepsilon)\,,$$
$$\langle d^{n+1}\varepsilon\varepsilon|H|d^{n+2}\varepsilon\varepsilon\varepsilon\rangle=\sqrt{3}\,V(\varepsilon)\,,$$
$$\langle d^{n+1}\varepsilon\varepsilon|H|d^{n+2}\varepsilon\varepsilon\varepsilon'\rangle=V(\varepsilon')\qquad(\text{etc.})\,,$$
$$\langle d^{n+1}\varepsilon\varepsilon'|H|d^{n+2}\varepsilon\varepsilon\varepsilon'\rangle=\sqrt{2}\,V(\varepsilon)\qquad(\text{etc.})\,,$$
$$\langle d^{n+1}\varepsilon\varepsilon'|H|d^{n+2}\varepsilon\varepsilon'\varepsilon''\rangle=V(\varepsilon'')\qquad(\text{etc.})\,.\qquad(\text{A}\cdot 5)$$

Appendix B

If other channels for photoemission are present besides of the d channel the relationship between the local d-density of states and the observed photoemission spectrum is rather indirect. Van der Marel has studied this matter in detail for uncorrelated impurities[58] and has shown how to obtain (under certain model assumptions) the local d-density of states of the impurity from difference spectra. With respect to correlated systems one would at first glance expect that, if host photoemission is dominant, the spectral features are quite well described by the single particle dispersions of the host bands. However, because of the d-host band hybridization also in this case we are faced with a many-body problem and these many-body effects may have a profound influence on the spectral line shape, at least in the concentrated limit.

The two-hole Green's function method can be used to obtain some rigorous results for this problem. Equation (3·5) can be rewritten as

$$G^<_{\text{tot}}(\gamma mm', z)=|A_d(k_F)|^2G^<_{dd}(\gamma mm', z)$$
$$+\int d\varepsilon\{A_L{}^*(k_F,\varepsilon)A_d(k_F)G^<_{\varepsilon d}(\gamma mm', z)$$
$$+A_L(k_F,\varepsilon)A_d{}^*(k_F)G^<_{d\varepsilon}(\gamma mm', z)\}$$
$$+\int d\varepsilon d\varepsilon' A_L{}^*(k_F,\varepsilon)A_L(k_F,\varepsilon')G^<_{\varepsilon\varepsilon'}(\gamma mm', z)+G_m{}^{NB}(z)\delta_{mm'}\qquad(\text{B}\cdot 1)$$

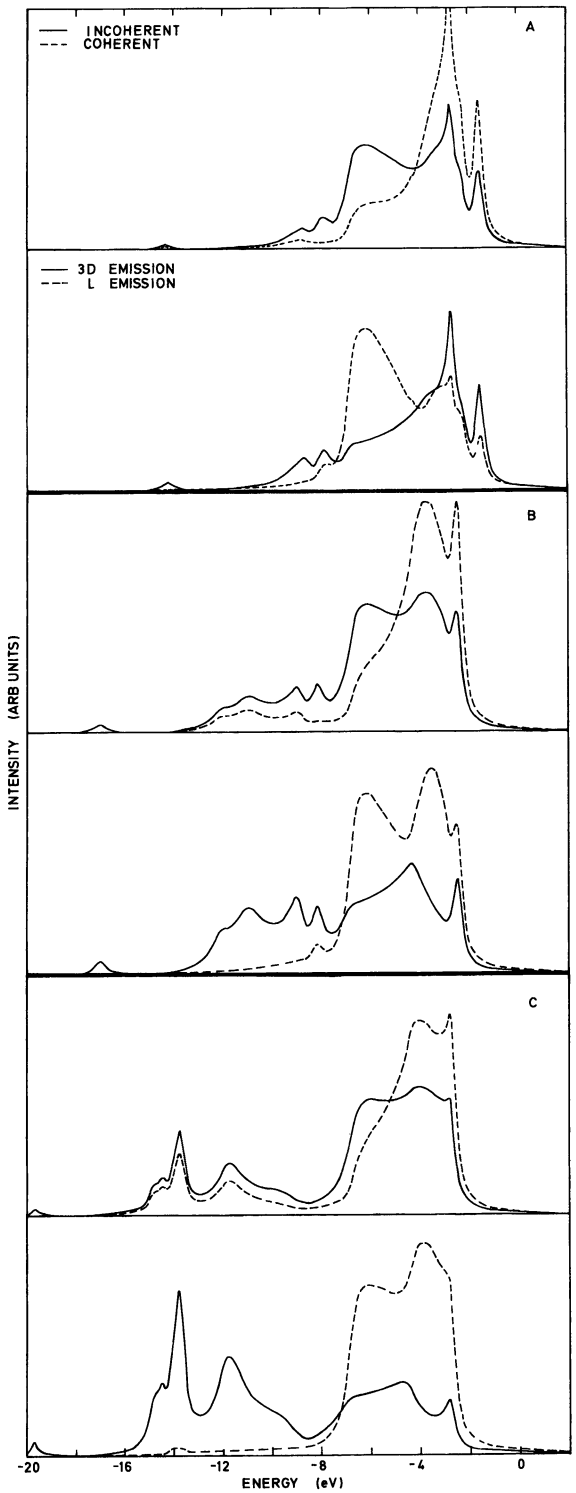

Fig. 11. Competition between $3d$ and ligand p emission for different photoemission mechanisms in the quasi-isolated impurity model. In (A)~(C) the Racah A is 3, 6 and 9 eV, respectively.

with $G^{<}_{dd}$ given by (3·8) and

$$G^{<}_{\varepsilon\varepsilon'}(\gamma mm', z)=\langle\Phi_0;\Gamma|c^{+}_{\varepsilon m}\hat{G}c_{\varepsilon' m'}|\Phi_0;\Gamma\rangle\,,$$
$$G^{<}_{\varepsilon d}(\gamma mm', z)=\langle\Phi_0;\Gamma|c^{+}_{\varepsilon m}\hat{G}d_m|\Phi_0;\Gamma\rangle\,. \tag{B·2}$$

In Eq. (B·1) we have also included a contribution to the photoemission of ligand electrons which are non-bonding with respect to the d-shell of the impurity ($G_m^{NB}(z)$, $m=m_l, m_s$; $l\neq 2$). Along the same lines as for $G^{<}_{dd}$ we find

$$G^{<}_{\varepsilon\varepsilon'}(\gamma mm', z)=g_\varepsilon^{\varepsilon'}(m, z)\delta_{mm'}+g_\varepsilon^{d}(m, z)\langle n_d\rangle T^{\gamma m'}_{\gamma m}g_d^{\varepsilon'}(m', z)\,,$$
$$G^{<}_{\varepsilon d}(\gamma mm', z)=g_\varepsilon^{d}(m, z)\delta_{mm'}+g_\varepsilon^{d}(m, z)\langle n_d\rangle T^{\gamma m'}_{\gamma m}g_d^{d}(m, z)\,. \tag{B·3}$$

The one-hold Green's functions appearing in Eq. (B·3) are given in the Anderson model by

$$g_\varepsilon^{\varepsilon'}(m, z)=g_\varepsilon(z)\delta(\varepsilon-\varepsilon')+g_\varepsilon(z)\,V_m^{*}(\varepsilon)g_d^{d}(m, z)\,V_m(\varepsilon')g_{\varepsilon'}(z)\,,$$
$$g_\varepsilon^{d}(m, z)=g_d^{d}(m, z)\,V_m^{*}(\varepsilon)g_\varepsilon(z)\,,$$
$$g_\varepsilon(z)=(z-\delta+\Delta+\varepsilon)^{-1}\,. \tag{B·4}$$

Combining Eqs. (B·1)~(B·4) finally yields

$$G^{<}_{\mathrm{tot}}(\gamma mm', z)=c\tilde{A}^{*}(m, z)\tilde{A}(m', z)G^{<}_{dd}(\gamma mm', z)+\tilde{B}(m, z)\delta_{mm'}+G_m^{NB}(z)\delta_{mm'}\,, \tag{B·5}$$

where

$$\tilde{A}(m, z)=A_d(k_F)+\int d\varepsilon A_L(k_F, \varepsilon)\,V_m^{*}(\varepsilon)g_\varepsilon(z)\,,$$
$$\tilde{B}(m, z)=\int d\varepsilon|A_L(k_F, \varepsilon)|^2 g_\varepsilon(z)\,. \tag{B·6}$$

In Eq. (B·5) we also include the impurity concentration (c). By setting $V_m(\varepsilon)=V_m\rho^{1/2}(\varepsilon)$ and $A_L(\varepsilon, k_F)=A_L(k_F)\rho^{1/2}(\varepsilon)$ Eq. (B·6) are further simplified to

$$\tilde{A}(m, z)=A_d(k_F)+A_L(k_F)\,V_m^{*}\Gamma(z-\delta+\Delta)\,,$$
$$\tilde{B}(m, z)=|A_L(k_F)|^2\Gamma(z-\delta+\Delta) \tag{B·7}$$

with $\Gamma(z)$ defined in Eq. (3·16). With these definitions A_d and A_L can be compared to atomic (d and p) ionization amplitudes.

In order to mimic the concentrated systems we set $c=1$ in Eq. (B·5) and to account for G^{NB} we assume that we have for each cation twelve anion bands of different m, corresponding with the 12 p orbitals on the nearest-neighbour ligands in the cluster calculation of Cu dihalides.[25] Ten of these are of d symmetry such that we have to add 2 non-bonding bands. Finally we note that Eq. (B·5) is only appropriate at relatively low kinetic energy. At high kinetic energy (>50 eV) the wavelength of the emitted electron becomes substantially smaller than the interatomic distance and the uncertainty in the real space positions of the atoms destroys the coherence between the different ionization channels (direct vs indirect transition model). In

terms of our calculation this means that terms proportional to $A_L^*(k_F)A_d(k_F)$ and $A_L(k_F)A_d^*(k_F)$ in Eq. (B·5) have to be neglected for $E(k_F)>50$ eV.[25]

In Fig. 11 we show results obtained from Eq. (B·5) for the same parameter range as in Fig. 5 (we omitted $A=0$ eV). For each parameter set we compare p-emission only ($A_L=1$, $A_d=0$) $3d$-emission only ($A_L=0$, $A_d=1$) and both p and $3d$ emission ($A_L=1$, $A_d=-1$) including-('coherent') and excluding ('incoherent') the interference terms. Focussing first on the p-emission only it is seen that this is mainly concentrated in the valence band region. Although the satellite barely shows up in this spectrum, the shape of the valence band still depends rather strongly on the magnitude of U, which is not surprising because of the strong hybridization with the d states. This is a subtle problem, as can be illustrated by a simple cluster calculation. Taking a cluster with spin degenerate 'd' and 'L' orbitals which are hybridized ($T=\langle d|H|L\rangle$) and assuming that these orbitals are at the same energy we obtain for $U=0$ a bonding ($\varphi_B=(|d\rangle+|L\rangle)/\sqrt{2}$) and an antibonding ($\varphi_A=(|d\rangle-|L\rangle)/\sqrt{2}$) molecular orbital. In the ground state of the cluster we take a single up spin hole in the antibonding level. Considering the 'majority spin' photoemission we then find two lines with equal intensity in the spectrum, corresponding with the antibonding (at $E=0$) and bonding (at $E=-2|T|$) orbitals. It is instructive to consider the $U\to\infty$ limit where at least the influence of the 'd^0' configuration on the 'valence band' region is removed. The two-hole eigenstates of the cluster are found to be (see also Ref. 25))

$$
\begin{aligned}
&|\varphi_1\rangle=(|L_\uparrow d_\downarrow\rangle+|d_\uparrow L_\downarrow\rangle+\sqrt{2}|L_\uparrow L_\downarrow\rangle)/2\,,\\
&|\varphi_2\rangle=(|L_\uparrow d_\downarrow\rangle-|d_\uparrow L_\downarrow\rangle)/\sqrt{2}\,,\\
&|\varphi_3\rangle=(|L_\uparrow d_\downarrow\rangle+|d_\uparrow L_\downarrow\rangle-\sqrt{2}|L_\uparrow L_\downarrow)/2\,,\\
&|\varphi_4\rangle=|d_\uparrow d_\downarrow\rangle\,. \qquad \text{(B·8)}
\end{aligned}
$$

The relative positions of the valence band states ($|\varphi_1\rangle$, $|\varphi_2\rangle$, $|\varphi_3\rangle$) are now $+\sqrt{2}T$, 0 and $-\sqrt{2}T$ and for the intensities of these lines in the $L_\downarrow$ spectrum we find $I_1=(1-1/\sqrt{2})^2/4$, $I_2=1/4$ and $I_3=(1+1/\sqrt{2})^2/4$. This example shows the untrivial nature of the problem and it gives some feeling why the valence band is (also for large U) strongly distorted while also intensity is found below the bottom of the valence band where the '$S(z)$' two-hole states are located.

Considering the interplay of d- and p-emission it is seen that p-emission favours strongly the intensity in the valence band region. This is because the d-weight is spread over the full spectral range while the p weight is concentrated in the valence band region. In the incoherent case the p and d only spectra are simply added but in the coherent case interference terms are present. One effect of this interference is that the satellite-main intensity ratio is changed. This effect is however minor and the major effect is that the shape of the valence band is strongly changed. In our example the valence band seems to narrow for opposite phases of A_L and A_d and to broaden[48] if the phases are the same. It is expected that, because of the changes in phase and magnitude of the photoemission cross sections, the line shape of the ligand band will be strongly photon-energy dependent at relatively low energy. This may explain the vastly different main line shapes observed in the He (I) and He (II) spectra

of $CuCl_2$[25] and the similar behaviour in the EDC's of other transition metal compounds in the synchrotron study by Kakizaki et al.[49]

References

1) N. F. Mott, Proc. Phys. Soc. London **A62** (1949), 416.
2) J. Hubbard, Proc. R. Soc. London **A277** (1964), 237; **281** (1964), 401.
3) S. Sugano, Y. Tanabe and A. Kamimura, *Multiplets of Transition Metal Ions in Crystals* (Academic Press, N. Y., 1970).
4) C. Haas, Crit. Rev. Solid State Sciences **1** (1970), 47.
5) J. A. Wilson, Adv. Phys. **21** (1972), 143.
6) G. A. Sawatzky and J. W. Allen, Phys. Rev. Lett. **53** (1984), 2339.
7) S. Hüfner, J. Osterwalder, T. Riesteren and F. Hulliger, Solid State Commun. **52** (1984), 793.
8) D. Adler and J. Feinleib, Phys. Rev. **B2** (1970), 3112.
   B. Koiller and L. M. Falicov, J. of Phys. **C7** (1974), 299.
9) R. J. Powell and W. E. Spicer, Phys. Rev. **B2** (1970), 2182.
   K. W. Blazy, Physica (Utrecht) **89B** (1977), 47.
10) P. A. Lee, T. M. Rice, J. W. Serene, L. J. Sham and J. W. Wilkins, Comments on Cond. Mat. Phys. **12** (1986), 99.
   O. Gunnarsson and K. Schönhammer, *Handbook on the Physics and Chemistry of Rare Earth*, ed. K. Gschneider, L. Eyring and S. Hüfner (North-Holland, Amsterdam), vol. 10.
   J. W. Allen, S. -J. Oh, O. Gunnarsson, K. Schönhammer, M. B. Maple, M. S. Torikachvili and I. Lindau, Adv. Phys. **35** (1986), 275.
11) R. H. Victora and L. M. Falicov, Phys. Rev. Lett. **55** (1985), 1140.
12) B. W. Veal and A. P. Paulakis, Phys. Rev. Lett. **51** (1983), 1995.
   J. Zaanen, C. Westra and G. A. Sawatzky, Phys. Rev. **B33** (1986), 8060.
   G. van der Laan, J. Zaanen, G. A. Sawatzky, R. Karnatak and J. -M. Esteva, Phys. Rev. **B33** (1986), 4253.
   J. Park, S. Ryu, M. Han and S. -J. Oh, Phys. Rev. **B65** (1987), 1262.
13) In *Core Level Spectroscopy in Condensed Systems*, ed. J. Kanamori and A. Kotani (Springer Solid State Series 81, 1988).
   K. Okada and A. Kotani, J. Phys. Soc. Jpn. **58** (1989), 2578.
14) J. Zaanen, G. A. Sawatzky and J. W. Allen, J. Magn. Magn. Mater. **54-57** (1986), 607.
15) J. F. Lang, Y. Bear and P. A. Cox, J. of Phys. **F11** (1981), 121.
16) O. Gunnarsson and K. Schönhammer, Phys. Rev. **B28** (1983), 4315.
17) O. Gunnarsson and K. Schönhammer, Phys. Rev. **B31** (1985), 4815.
18) L. F. Mattheiss, Phys. Rev. **B5** (1972), 290.
   T. Oguchi, K. Terakura and A. R. Williams, Phys. Rev. **B28** (1983), 6443; **B30** (1984), 4734.
   R. Coehoorn, Thesis, University of Groningen (1985).
19) G. K. Wertheim and S. Hüfner, Phys. Rev. Lett. **28** (1972), 1028.
20) G. K. Wertheim, H. J. Guggenheim and S. Hüfner, Phys. Rev. Lett. **30** (1973), 1050.
21) K. S. Kim, J. Elec. Spectr. Rel. Phen. **3** (1974), 217.
22) D. E. Eastman and J. F. Freeouf, Phys. Rev. Lett. **34** (1975), 395.
23) B. H. Brandow, Adv. Phys. **26** (1977), 651.
24) L. C. Davis, J. Appl. Phys. **59** (1986), R25.
25) G. van der Laan, Solid State Commun. **42** (1982), 165.
26) A Fujimori and F. Minami, Phys. Rev. **B30** (1984), 957.
27) J. M. McKay and V. E. Henrich, Phys. Rev. Lett. **53** (1984), 2343.
28) H. I. Sternberg, M. T. Johnson and H. P. Huges, J. of Phys. **C19** (1986), 2689.
29) Z. -X. Shen, C. K. Shih, O. Jepsen, W. E. Spicer, I. Lindau and J. W. Allen, Phys. Rev. Lett. **64** (1990), 2442.
   N. B. Brookes, D. S. -L. Law, D. R. Warburton, P. L. Wincott and G. Thornton, J. of Phys. Cond. Matt. **1** (1989), 4267.
30) J. Zaanen and G. A. Sawatzky, Can. J. Phys. **65** (1987), 1262.
31) J. Kanamori, Prog. Theor. Phys. **30** (1963), 275.

32) M. Cini, Solid State Commun. **24** (1977), 681.
G. A. Sawatzky, Phys. Rev. Lett. **39** (1977), 504.
V. Drchal and J. Kudrnovsky, Phys. Status Solidi **B114** (1982), 627.
33) M. Vos, D. van der Marel and G. A. Sawatzky, Phys. Rev. **B29** (1984), 3073.
34) P. Hedegard and B. Johannson, Phys. Rev. Lett. **52** (1984), 2168; Phys. Rev. **B31** (1985), 7749.
35) J. Zaanen, G. A. Sawatzky and J. W. Allen, Phys. Rev. Lett. **55** (1985), 418.
36) P. W. Anderson, Phys. Rev. **124** (1961), 41.
37) P. Thiry, D. Chandesris, J. Lecante, C. Guillot, R. Pinchaux and Y. Pêtroff, Phys. Rev. Lett. **43** (1979), 82.
38) H. W. Haak, Thesis, University of Groningen (1982).
39) K. A. Chao, J. Spalek and A. M. Oleś, J. of Phys. **C10** (1977), L271; Phys. Rev. **B18** (1978), 3453.
40) J. C. W. Folmer and F. Jellinek, J. Less-Common Metals **76** (1980), 153.
41) F. Jellinek, *M. T. P. International Review of Science, Inorganic Chemistry Series I* (Butterworths, London, 1972), vol. 5, p. 339.
42) J. S. Griffith, *The Theory of Transition Metal Ions* (Cambridge University, Cambridge, 1961).
43) G. J. Ballhausen, *Intr. to Ligand Field Theory* (McGraw-Hill, N. Y., 1962).
44) A. Zunger, *Solid State Physics **39***, ed. H. Ehrenreich and D. Turnbull (Academic Press, 1986) p. 276.
45) H. Eskes and G. A. Sawatzky, Phys. Rev. Lett. **61** (1988), 1415.
46) F. C. Zhang and T. M. Rice, Phys. Rev. **B37** (1988), 3759.
47) J. Zaanen and G. A. Sawatzky, Phys. Rev. **B33** (1986), 8074.
48) J. Zaanen, Thesis, University of Groningen (1986).
49) A. Kakizaki, K. Sugeno, T. Ishii, H. Sugawara, I. Nagakura and S. Shin, Phys. Rev. **B28** (1983), 1026.
50) S. J. Oh, J. W. Allen, I. Lindan and J. C. Mikkelsen, Phys. Rev. **B26** (1982), 4845.
51) O. Gunnarsson, O. K. Andersen, O. Jepsen and J. Zaanen, in *Core Level Spectroscopy in Condensed Systems*, ed. J. Kanamori and A. Kotani (Springer Solid State Sciences 81, 1987), p. 82.
52) C. R. Ronda, Thesis, University of Groningen (1986).
53) S. Hüfner, Solid State Commun. **53** (1985), 707.
54) J. Zaanen and G. A. Sawatzky, J. of Solid State Chem. (in press).
55) N. B. Brandt and V. V. Moshchalkov, Adv. Phys. **33** (1984), 193.
56) G. J. M. Janssen, Thesis, University of Groningen (1986).
57) M. R. Norman and A. J. Freeman, Phys. Rev. **B33** (1986), 8896.
58) D. van der Marel, C. Westra, G. A. Sawatzky and F. U. Hillebrecht, Phys. Rev. **B31** (1985), 1936.